Maier, B., Gluba, W., Bernier, B., Turner, T., Mohammad, K., Guise, T., Sutherland, A., Thorner, M., and Scrable, H. (2004). Modulation of mammalian life span by the short isoform of p53. Genes Dev. *18*, 306–319.

Marino, S., Vooijs, M., van Der Gulden, H., Jonkers, J., and Berns, A. (2000). Induction of medulloblastomas in p53-null mutant mice by somatic inactivation of Rb in the external granular layer cells of the cerebellum. Genes Dev. *14*, 994–1004.

Meek, D.W. (2009). Tumour suppression by p53: a role for the DNA damage response? Nat. Rev. Cancer *9*, 714–723.

Minamino, T., and Komuro, I. (2007). Vascular cell senescence: contribution to atherosclerosis. Circ. Res. *100*, 15–26.

Minamino, T., and Komuro, I. (2008). Vascular aging: insights from studies on cellular senescence, stem cell aging, and progeroid syndromes. Nat. Clin. Pract. Cardiovasc. Med. *5*, 637–648.

Minamino, T., Orimo, M., Shimizu, I., Kunieda, T., Yokoyama, M., Ito, T., Nojima, A., Nabetani, A., Oike, Y., Matsubara, H., et al. (2009). A crucial role for adipose tissue p53 in the regulation of insulin resistance. Nat. Med. *15*, 1082–1087.

Nemoto, S., Razeghi, P., Ishiyama, M., De Freitas, G., Taegtmeyer, H., and Carabello, B.A. (2005). PPAR-gamma agonist rosiglitazone ameliorates ventricular dysfunction in experimental chronic mitral regurgitation. Am. J. Physiol. Heart Circ. Physiol. *288*, H77–H82.

Neubauer, S. (2007). The failing heart—an engine out of fuel. N. Engl. J. Med. *356*, 1140–1151.

Nikolaidis, L.A., Sturzu, A., Stolarski, C., Elahi, D., Shen, Y.T., and Shannon, R.P. (2004). The development of myocardial insulin resistance in conscious dogs with advanced dilated cardiomyopathy. Cardiovasc. Res. *61*, 297–306.

Opie, L.H. (2004). The metabolic vicious cycle in heart failure. Lancet *364*, 1733–1734.

Ouchi, N., Parker, J.L., Lugus, J.J., and Walsh, K. (2011). Adipokines in inflammation and metabolic disease. Nat. Rev. Immunol. *11*, 85–97.

Packer, M., Coats, A.J., Fowler, M.B., Katus, H.A., Krum, H., Mohacsi, P., Rouleau, J.L., Tendera, M., Castaigne, A., Roecker, E.B., et al; Carvedilol Prospective Randomized Cumulative Survival Study Group. (2001). Effect of carvedilol on survival in severe chronic heart failure. N. Engl. J. Med. *344*, 1651–1658.

Packer, M., Fowler, M.B., Roecker, E.B., Coats, A.J., Katus, H.A., Krum, H., Mohacsi, P., Rouleau, J.L., Tendera, M., Staiger, C., et al; Carvedilol Prospective Randomized Cumulative Survival (COPERNICUS) Study Group. (2002). Effect of carvedilol on the morbidity of patients with severe chronic heart failure: results of the carvedilol prospective randomized cumulative survival (COPERNICUS) study. Circulation *106*, 2194–2199.

Poole-Wilson, P.A., Swedberg, K., Cleland, J.G., Di Lenarda, A., Hanrath, P., Komajda, M., Lubsen, J., Lutiger, B., Metra, M., Remme, W.J., et al; Carvedilol Or Metoprolol European Trial Investigators. (2003). Comparison of carvedilol and metoprolol on clinical outcomes in patients with chronic heart failure in the Carvedilol Or Metoprolol European Trial (COMET): randomised controlled trial. Lancet *362*, 7–13.

Royds, J.A., and Iacopetta, B. (2006). p53 and disease: when the guardian angel fails. Cell Death Differ. *13*, 1017–1026.

Ryan, K.M., Ernst, M.K., Rice, N.R., and Vousden, K.H. (2000). Role of NF-kappaB in p53-mediated programmed cell death. Nature *404*, 892–897.

Sano, M., Minamino, T., Toko, H., Miyauchi, H., Orimo, M., Qin, Y., Akazawa, H., Tateno, K., Kayama, Y., Harada, M., et al. (2007). p53-induced inhibition of Hif-1 causes cardiac dysfunction during pressure overload. Nature *446*, 444–448.

Schenk, S., Saberi, M., and Olefsky, J.M. (2008). Insulin sensitivity: modulation by nutrients and inflammation. J. Clin. Invest. *118*, 2992–3002.

Schnabel, P., Maack, C., Mies, F., Tyroller, S., Scheer, A., and Böhm, M. (2000). Binding properties of beta-blockers at recombinant beta1-, beta2-, and beta3-adrenoceptors. J. Cardiovasc. Pharmacol. *36*, 466–471.

Sharma, N., Okere, I.C., Duda, M.K., Chess, D.J., O'Shea, K.M., and Stanley, W.C. (2007). Potential impact of carbohydrate and fat intake on pathological left ventricular hypertrophy. Cardiovasc. Res. *73*, 257–268.

Shimizu, I., Minamino, T., Toko, H., Okada, S., Ikeda, H., Yasuda, N., Tateno, K., Moriya, J., Yokoyama, M., Nojima, A., et al. (2010). Excessive cardiac insulin signaling exacerbates systolic dysfunction induced by pressure overload in rodents. J. Clin. Invest. *120*, 1506–1514.

Suskin, N., McKelvie, R.S., Burns, R.J., Latini, R., Pericak, D., Probstfield, J., Rouleau, J.L., Sigouin, C., Solymoss, C.B., Tsuyuki, R., et al. (2000). Glucose and insulin abnormalities relate to functional capacity in patients with congestive heart failure. Eur. Heart J. *21*, 1368–1375.

Tenenbaum, A., Motro, M., Fisman, E.Z., Leor, J., Freimark, D., Boyko, V., Mandelzweig, L., Adler, Y., Sherer, Y., and Behar, S. (2003). Functional class in patients with heart failure is associated with the development of diabetes. Am. J. Med. *114*, 271–275.

Torp-Pedersen, C., Metra, M., Charlesworth, A., Spark, P., Lukas, M.A., Poole-Wilson, P.A., Swedberg, K., Cleland, J.G., Di Lenarda, A., Remme, W.J., and Scherhag, A.; COMET investigators. (2007). Effects of metoprolol and carvedilol on pre-existing and new onset diabetes in patients with chronic heart failure: data from the Carvedilol Or Metoprolol European Trial (COMET). Heart *93*, 968–973.

Tuunanen, H., Engblom, E., Naum, A., Någren, K., Hesse, B., Airaksinen, K.E., Nuutila, P., Iozzo, P., Ukkonen, H., Opie, L.H., and Knuuti, J. (2006). Free fatty acid depletion acutely decreases cardiac work and efficiency in cardiomyopathic heart failure. Circulation *114*, 2130–2137.

Tyner, S.D., Venkatachalam, S., Choi, J., Jones, S., Ghebranious, N., Igelmann, H., Lu, X., Soron, G., Cooper, B., Brayton, C., et al. (2002). p53 mutant mice that display early ageing-associated phenotypes. Nature *415*, 45–53.

Vousden, K.H., and Lane, D.P. (2007). p53 in health and disease. Nat. Rev. Mol. Cell Biol. *8*, 275–283.

Vousden, K.H., and Prives, C. (2009). Blinded by the Light: The Growing Complexity of p53. Cell *137*, 413–431.

Vousden, K.H., and Ryan, K.M. (2009). p53 and metabolism. Nat. Rev. Cancer *9*, 691–700.

Weisberg, S.P., McCann, D., Desai, M., Rosenbaum, M., Leibel, R.L., and Ferrante, A.W., Jr. (2003). Obesity is associated with macrophage accumulation in adipose tissue. J. Clin. Invest. *112*, 1796–1808.

Witteles, R.M., and Fowler, M.B. (2008). Insulin-resistant cardiomyopathy clinical evidence, mechanisms, and treatment options. J. Am. Coll. Cardiol. *51*, 93–102.

Young, M.E., McNulty, P., and Taegtmeyer, H. (2002). Adaptation and maladaptation of the heart in diabetes: Part II: potential mechanisms. Circulation *105*, 1861–1870.

Zeng, L., Wu, G.Z., Goh, K.J., Lee, Y.M., Ng, C.C., You, A.B., Wang, J., Jia, D., Hao, A., Yu, Q., and Li, B. (2008). Saturated fatty acids modulate cell response to DNA damage: implication for their role in tumorigenesis. PLoS ONE *3*, e2329.

Journal of Molecular and Cellular Cardiology 51 (2011) 821–829

Contents lists available at SciVerse ScienceDirect

Journal of Molecular and Cellular Cardiology

journal homepage: www.elsevier.com/locate/yjmcc

Original article

Heat shock transcription factor 1 protects heart after pressure overload through promoting myocardial angiogenesis in male mice

Yunzeng Zou [a,b,1,*], Jiming Li [a,1,2], Hong Ma [a,1,3], Hong Jiang [a,1], Jie Yuan [b,1], Hui Gong [b,1], Yanyan Liang [a], Aili Guan [a], Jian Wu [b], Lei Li [b], Ning Zhou [a], Yuhong Niu [a], Aijun Sun [a,b], Akira Nakai [c], Ping Wang [d], Hiroyuki Takano [d], Issei Komuro [d], Junbo Ge [a,b,*]

[a] *Shanghai Institute of Cardiovascular Diseases, Zhongshan Hospital, Fudan University, Shanghai 200032, China*
[b] *Institutes of Biomedical Sciences, Fudan University, Shanghai 200032, China*
[c] *Department of Biochemistry and Molecular Biology, Yamaguchi University School of Medicine, Ube, Japan*
[d] *Department of Cardiovascular Science and Medicine, Chiba University Graduate School of Medicine, Chiba, Japan*

ARTICLE INFO

Article history:
Received 11 April 2011
Received in revised form 30 July 2011
Accepted 30 July 2011
Available online 7 August 2011

Keywords:
Angiogenesis
Cardiac hypertrophy
Endothelial cell
HSF1
Pressure overload

ABSTRACT

Heat shock transcription factor 1 (HSF1) plays an important role not only in excise-induced cardiac hypertrophy but also in protection against pressure overload-induced cardiac dysfunction. However, the mechanism is not completely understood. We here elucidate the potential mechanisms by which HSF1 protects against pressure overload-induced cardiac remodeling and dysfunction. A sustained constriction of transverse aorta (TAC) was imposed to *HSF1* transgenic (TG), knockout (KO) and their littermate wild type (WT) male mice. Four weeks later, adaptive responses to TAC, such as cardiac hypertrophy, contractility and angiogenesis evaluated by echocardiography, catheterization, coronary perfusion pressure and immunohistochemistry were well preserved in TG but not in KO compared with WT mice. An angiogenesis inhibitor TNP-470 abrogated all these adaptive responses in TG mice, while cardiac transfection of *VEGF* with *angiopoietin-1* rescued the broken heart in KO mice. In response to TAC, p53 was downregulated and hypoxia-inducing transcription factor-1 (HIF-1) was upregulated not only in the heart but also in the cultured cardiac endothelial cells (EC) of TG mice as compared to WT mice whereas these changes became opposite in KO mice. A small interfering RNA (siRNA) of *HIF-1* but not a *p53* gene impaired the adaptive responses of the heart and EC in TG mice, and a siRNA of *p53* but not a *HIF-1* gene significantly reversed the heart and EC disorders in KO mice after TAC. We conclude that HSF1 promotes cardiac angiogenesis through suppression of p53 and subsequent upregulation of HIF-1 in endothelial cells during chronic pressure overload, leading to the maintenance of cardiac adaptation.

1. Introduction

Cardiac hypertrophy is an adaptive response of the heart to increase work load [1,2]. At the beginning, cardiac hypertrophy is beneficial to maintain cardiac output by reducing wall stress, but it becomes maladaptive in the chronic phase, resulting in heart failure [3]. However, physiological cardiac hypertrophy could maintain normal function without progression to heart failure [4,5]. Recently, it has been reported that heat shock transcription factor 1 (HSF1), which regulates heat shock proteins' (HSPs) expression and protects against ischemic injury of the heart, plays a critical role in adaptive response of the heart to exercise in mice [6]. In this study, expression of *HSF1* and its target molecule HSPs were significantly upregulated in the heart during exercises, and reduction of *HSF1* expression in the heart declined the cardiac adaptation. Moreover, overexpression of *HSF1* in the heart preserved cardiac function, while reduction of *HSF1* expression impaired early adaptive response to acute pressure overload [6].

Although the beneficial effects of HSF1 were attributed to decreases of cardiomyocyte death and myocardial fibrosis [6], the cellular and molecular mechanisms remain largely unclear. Additionally, although it was indicated that HSF1 was not upregulated in the heart by a chronic pressure overload [6] and that HSF1 activation and HSP72 gene transcriptional competence during simulated exercise are linked to elevated heart temperature and are not a direct function of increased cardiac workload [7], it has also been indicated that transcription of HSPs by HSF1 may be directly activated by mechanical

* Corresponding authors at: Shanghai Institute of Cardiovascular Diseases, Zhongshan Hospital, Fudan University, 180 Feng Lin Road, Shanghai 200032, China. Tel./fax: +86 21 5423 7969.
E-mail addresses: zou.yunzeng@zs-hospital.sh.cn (Y. Zou), jbge@zs-hospital.sh.cn (J. Ge).
[1] These authors contributed equally to this work.
[2] Present address: Department of Cardiology, Shanghai East Hospital, Tongji University, Shanghai, China.
[3] Present address: Department of Cardiology, 2nd Affiliated Hospital Zhejiang University College of Medicine, Hangzhou, China.

0022-2828/$ – see front matter © 2011 Elsevier Ltd. All rights reserved.
doi:10.1016/j.yjmcc.2011.07.030

stress in the heart in both *in vitro* and *in vivo* models, which plays an important role in myocardial protection against cardiac overload [8] and that mechanical stretch-stimulated activation of HSF1 in rat heart is mediated by stretch-activated ion channels [9]. The reason for these discrepancies is still unexplained.

Recently, we observed that cardiac angiogenesis induced by hypoxia-inducing transcription factor (HIF)-1 is crucially involved in the adaptive mechanism of cardiac hypertrophy and that impairment of cardiac angiogenesis by p53 accumulation induces transition of the adaptive cardiac hypertrophy to heart failure during pressure overload [10]. However, the mechanism of how pressure overload induces the changes of HIF-1 and p53 expression is not yet answered by the study. It has been indicated that expression of HSPs, in particular that of HSP70 and HSP90, is required to maintain HIF-1 stabilization [11], and that HSF1 transcription is upregulated during hypoxia due to direct binding by HIF-1 to HIF-1 response elements in an HSF intron, which is necessary for full HSP induction during hypoxia and reoxygenation [12]. On the other hand, p53 has been known to interact with some members of the HSF1 pathway including HSP70 and HSP90 and HSP90 has been shown to play an important role in p53 transcriptional activities [13–15]. All of these strongly suggest that there is a relationship between HSF1/HSPs-induced cardiac protection and p53/HIF-regulated angiogenesis.

In the present study, by using *HSF1* transgenic (TG), knockout (KO) and their littermate wild type (WT) mice, we examined how HSF1 could preserve adaptation of the heart during a chronic pressure overload.

2. Materials and methods

2.1. Mice, pressure overload model and Langendorff perfusion

HSF1 TG and KO mice were generated as previously described [16,17]. In order to exclude the interference of sex hormone undulation, twelve-week-old male TG, KO and their littermate male WT mice were used [18,19]. Strong pressure overload was imposed on the heart of mice by constriction of transverse aorta (TAC) [6,10,20]. Blood pressure (BP) and heart rate (HR) were measured using a Millar 1.4 F micronanometer catheter. The transducer was connected to Power Laboratory system (Supplementary Methods). Control mice before operation and mice at 2 and 4 weeks after sham or TAC operation were subjected to hemodynamic measurement, and those with elevation of BP by 40–50 mmHg after TAC or without BP elevation after sham operation in comparing with control mice were enclosed in analyses (Supplementary Tables 1 and 2). Isolation of mouse heart and Langendorff perfusion were performed as previous described [21] with some modifications (Supplementary Methods). All animal experimental protocols in the Guide for the Care and Use of Laboratory Animals (NIH publication no. 85–23, 1996) were complied with and were approved by the Animal Care and Use Committee at Fudan University.

2.2. Echocardiography

Transthoracic echocardiography was performed using an animal specific instrument (VisualSonics Vevo770, VisualSonics Inc.) [6,10,20,22]. Mice were anesthetized by isoflurane and M-mode images were recorded. All measurements were carried out by three experienced persons who were unaware of the identities of the experimental groups (Supplementary Methods).

2.3. cDNA constructs and transfection of adenoviral vectors

Construction of adenoviral vectors encoding *VEGF*, angiopoietin-1 (*Ang-1*), *HIF-1* and *p53* has been previously described [10]. Small interfering RNA (siRNA) of *HIF-1* and *p53*, and their scramble sequences were synthesized by PCR based method. These constructs were inserted into adenoviral vectors (Invitrogen). Transfection of adenoviral vectors encoding *HIF-1*, *p53* and their siRNAs into cultured cells and infusion of these genes into myocardium (10^9 pfu) were performed as reported previously (Supplementary Methods) [10]. In the present study, in order to induce sufficient angiogenesis, *VEGF* and *Ang1* have always been applied in combination since the angiogenesis by single molecule alone was less than the combination of the two molecules (paper in preparation and data not shown). Efficacy of adenoviral vector transfection into myocardium evaluated by an X-gal staining of LacZ vector was >50%, and injection of the siRNA induced significant knockdown (>50%) of HIF-1 and p53 proteins (Supplementary Figs. 1 and 2).

2.4. Reverse transcription-polymerase chain reaction (RT-PCR) analysis

Total RNA was isolated from heart tissues or cells using TRIzol reagent (Invitrogen). Expression of relative mRNA levels was evaluated using RT-PCR (Supplementary Methods). The PCR products were subject to electrophoresis on 1.5% agarose gels.

2.5. Isolation and culture of adult cardiac myocytes and endothelial cells of mice

Cardiac myocytes (CM) and endothelial cells (EC) were prepared from hearts of adult WT, TG and KO mice as described previously [20]. The cells were cultured in silicone dishes at a density of 1×10^5 cells/cm^2 [20,23] and in 100 mm dishes at a density of 5×10^4 cells/cm^2 to grow to sub-confluence (Supplementary Methods). The 2–3 passages of EC were used for vascular formation and transfection experiments.

2.6. Microvascular formation experiments

After 2–3 passages of culture, the EC were implanted onto the matrigel (BD Inc.) in plates at a density of 5×10^4 cells/well and grown for 18 h. Some of EC were subjected to a mechanical stretch for 60 min before the implantation. The capillary formation was observed under a microscope and quantified by calculating the total numbers of tube-like structures in whole well (Supplementary Methods).

2.7. Histological analysis

Heart tissues were fixed in 10% formalin and embedded in paraffin or frozen in cryomolds, sectioned at 4 μm thickness and stained with hematoxylin and eosin (H–E), Masson trichrome and anti vWF antibodies, respectively. For measurement, five random fields from each section were chosen and 5 sections from each heart were examined (Supplementary Methods).

2.8. Western blot analysis

Whole-cell lysates (30 μg) or nucleus extracts (20 μg) [22] were size fractionated by the SDS-polyacrylamide gel electrophoresis. Membranes (Millipore) were incubated with relative antibodies (Santa Cruz Biotechnology Inc.) (Supplementary Methods).

2.9. Statistics

Data are presented as mean ± S.E.M. Multiple group comparison was performed by one-way or two-way ANOVA followed by LSD procedure for comparison of means. Comparison between 2 groups under identical conditions was performed by the 2-tailed Student's *t* test. A value of $p<0.05$ was considered statistically significant.

3. Results

3.1. HSF1 promotes cardiac angiogenesis after pressure overload

The *HSF1* TG, KO and WT adult mice were apparently healthy, and there were no significant differences in body weight (BW), heart weight (HW), left ventricle (LV) wall thickness, LV cavity, LV ejection fraction (LVEF), BP and HR among the mice before TAC (Supplementary Tables 1 and 2; Supplementary Figs. 3 and 5) [6,24]. At 2 and 4 weeks after TAC, BP was similarly elevated in the three types of mice (Supplementary Table 2). Consistent with previous data, cardiac hypertrophy was more significantly formed in TG but less in KO mice (Supplementary Figs. 3, 4 and 5), cardiac contractility was well preserved in TG mice but impaired not only severely but also early in KO mice (Supplementary Fig. 3), LV remodeling including enlargement of end-diastolic LV inner diameter (LVIDd) and volume (LVVOLd), and intercellular collagen accumulation was mild in TG but significant in KO mice (Supplementary Figs. 3 and 4), and apoptotic cardiomyocytes were less in TG but more in KO heart (Supplementary Fig. 6) comparing to WT mice after TAC.

Here our data on microRNA analysis of hearts from *HSF1* TG and KO mice, which have been verified by realtime RT-PCR and Northern blotting, imply that HSF1 also has a role in promoting cardiac angiogenesis (Supplementary Fig. 7 and Supplementary Table 3). We therefore investigated the possible role of HSF1 as a cardiac angiogenesis-promoting factor during pressure overload. After TAC, the densities of vWF-positive vasculatures in myocardium were higher in TG mice but lower in KO ones than in WT mice (Fig. 1A). Also, cardiac HSP70 proteins were more in TG but less in KO than in WT mice (Supplementary Figs. 8A and 8B), consisting with the changes in angiogenesis. Additionally, neither TNP-470 treatment in *HSF1*-TG mice nor *VEGF* overexpression in the hearts of *HSF1*-KO mice could induce changes in HSP70 expression after TAC, suggesting that HSP70 expression is regulated by HSF1 but not by VEGF. To ask which cell type is related to promoting cardiac hypertrophy by HSF1, we separately cultured CM and microvascular EC of adult WT, TG and KO mice and subjected them to a mechanical stretch (MS). MS-evoked hypertrophic response was not significantly different among the three types of cultured CM (Supplementary Fig. 9), suggesting that HSF1 is not directly relative to CM hypertrophy. The abilities to form tube-like structures were not different among the three types of EC without MS (Fig. 1B). However, when MS was imposed to the cells, microvascular tubes were more formed by EC of TG mice (TG-EC) but less by EC of KO mice (KO-EC) as compared to EC of WT ones (WT-EC) (Fig. 1B). Also, the *VEGF* gene was more expressed either in myocardium or in EC of TG mice, but the expression was significantly less both in myocardium and EC of KO mice comparing to WT ones after stimulation with MS (Figs. 1C and D).

It is important to elucidate whether HSF-1-induced angiogenesis is of functional relevance. We performed Langendorff experiments to examine the coronary resistance in hearts of WT, TG and KO mice at 4 weeks after TAC (Fig. 1E). The results of coronary perfusion pressure showed that coronary resistance was lower in TG but higher in KO mice than in WT ones, associating with angiogenesis and VEGF expression. These data suggest that HSF-1-induced increase in cardiac angiogenesis is of functional relevance.

3.2. Angiogenesis contributes to the HSF1 effects on cardiac hypertrophy during pressure overload

To verify the role of angiogenesis in HSF1-related cardiac hypertrophy during pressure overload, we used an angiogenesis inhibitor, TNP-470 and angiogenesis promoters, *VEGF* and *Ang-1*. Inhibition of angiogenesis by TNP-470 significantly suppressed TAC-induced adaptive cardiac hypertrophy in *HSF1* TG mice (Figs. 2A, C, D and E), and introducing the *VEGF* with *Ang-1* genes into the heart of *HSF1* KO mice could reverse the maladaptive cardiac hypertrophy after TAC (Figs. 2B, C, D and F). Also, the abilities of *HSF1* TG-EC to form more microvessels after MS were significantly inhibited by TNP-470 (Figs. 2G and I), while the impairment of the vascular formation abilities of *HSF1* KO-EC were largely improved by transfection of the *VEGF* and *Ang-1* genes into these cells (Figs. 2H and I). These results indicate that HSF1 maintains adaptive cardiac hypertrophy during chronic pressure overload dependently on cardiac angiogenesis by EC.

3.3. siRNA of p53 but not HIF-1 gene injection reversed maladaptive cardiac hypertrophy in HSF1 KO mice

We next asked whether HIF-1 and p53 are involved in HSF1-regulated angiogenesis. There were no differences in basal gene expression of *HIF-1* and *p53* among the three types of mice (Supplementary Figs. 10A and 10B). Consisting with our previous study [10], expression of *HIF-1* gene in WT heart was increased at early phase and decreased from 2 weeks after TAC, and expression of *p53* gene was elevated from 2 weeks after TAC (Data not shown). However, expression of *HIF-1* gene was remained at a higher level in TG heart but fell into a very low level in KO heart compared with that in WT one at 4 weeks after TAC (Supplementary Fig. 10A). The expression of *p53* gene was not increased in TG heart until 4 weeks after TAC, but it expressed at a higher level in KO heart after TAC as compared to WT one (Supplementary Fig. 10B). Furthermore, in cultured EC, expression of *HIF-1* after MS was significantly increased in TG-EC but decreased in KO-EC (Supplementary Fig. 10C), while expression of *p53* after MS was significantly upregulated in KO-EC but downregulated in TG-EC (Supplementary Fig. 10D) when comparing to those in WT-EC. These results suggest that the expressions of *HIF-1* and *p53* are regulated by HSF1 in EC during pressure overload.

To further elucidate the roles of HIF-1 and p53 and their relationship in HSF1-preserved cardiac hypertrophy during pressure overload, we separately introduced a *HIF-1* gene or a siRNA of *p53* into myocardium of *HSF1* KO mice. TAC for 4 weeks caused down-regulation of HIF-1 and upregulation of p53 proteins in the myocardium, followed by a maladaptive cardiac hypertrophy in KO mice (Figs. 3A–G). Injection of the *HIF1* gene into the myocardium of KO mice did not induce the elevation of HIF-1 protein (Figs. 3A–C), nor reversed the maladaptive cardiac hypertrophy after TAC (Figs. 3D–G). Injection of the siRNA of *p53* did induce a decrease of p53 with an increase in HIF-1 proteins (Figs. 3A–C), accompanied by the improvement of maladaptive hypertrophy in KO mice after TAC (Figs. 3D–G). These data suggest that under the deficiency of HSF1, since there is a high level of p53 protein which could be activated by TAC, injection of an extrinsic *HIF-1* gene is unable to lead to an elevation of HIF-1 protein. However, inhibition of the intrinsic *p53* by a siRNA can liberate the HIF-1 protein, thereby prevents the maladaptive cardiac hypertrophy.

3.4. siRNA of HIF-1 but not p53 gene injection abrogated adaptive cardiac hypertrophy in HSF1 TG mice after TAC

We also injected a *p53* gene or a siRNA of *HIF-1* into the myocardium of *HSF1* TG mice. Introducing a *p53* gene into the myocardium of TG mice, which could not induce an increase in p53 protein (Figs. 4A–C), did not abrogate the adaptive cardiac hypertrophy after TAC (Figs. 4D–G), while injection of the siRNA of *HIF-1* gene, which could induce a downregulation of HIF-1 protein in the myocardium (Figs. 4A–C), resulted in a maladaptive cardiac hypertrophy after TAC (Figs. 4D–G). These results indicate that in *HSF1*-overexpressing heart, since injection of an extrinsic *p53* gene is unable to increase the p53 protein, it cannot decrease the HIF-1 protein and abrogate the adaptation of the heart after TAC. However, injection of a siRNA of *HIF-1* is capable of decreasing the HIF-1 protein, the injection can therefore lead to a maladaptive hypertrophy after TAC.

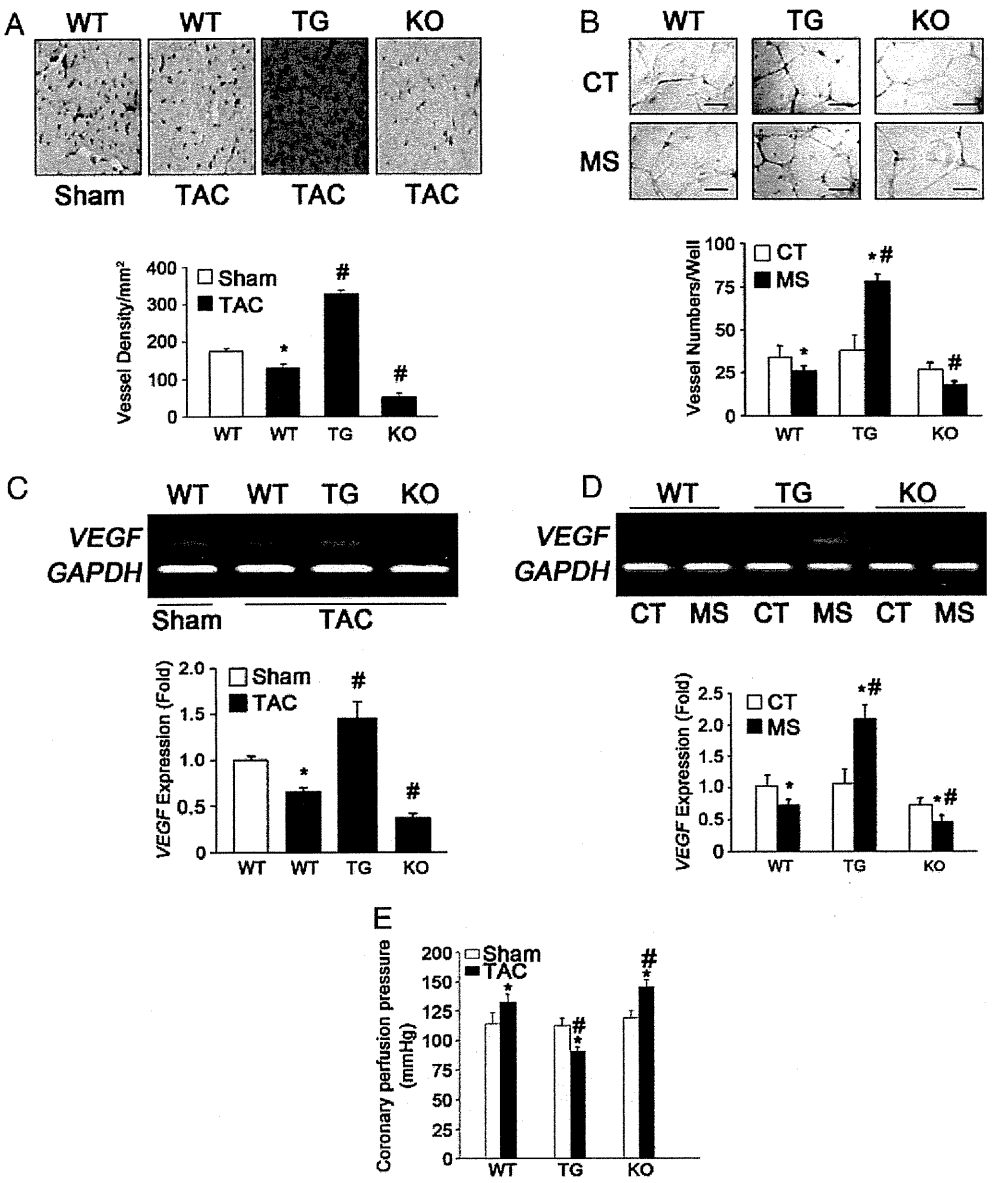

Fig. 1. Changes of vasculatures after mechanical stresses. (A) TAC was imposed to adult male WT, *HSF1* TG and KO mice for 4 weeks. Heart sections were stained by immunohistochemistry with an anti vWF antibody. Representative photographs are shown. Brown color indicates vWF-positive capillaries. vWF-positive vasculatures were calculated as the numbers per mm^2 area in LV wall. Data are expressed as mean ± S.E.M. of five hearts (n = 5). * $p<0.05$ *vs* WT mice with Sham; # $p<0.05$ *vs* WT with TAC. (B) Formation of vasculatures. EC were isolated from LV of the WT, TG and KO mice, and subjected to mechanical stretch (MS) or not (control, CT) for 60 min. Representative photographs of vessel-like tubes are shown (scale bar: 20 μm). Total vessels were counted in whole dish. Data are expressed as mean ± S.E.M. of three independent experiments (n = 3). * $p<0.05$ *vs* CT; # $p<0.05$ *vs* WT with MS. (C) RT-PCR analysis of *VEGF* expression in the heart of mice. (D) RT-PCR analysis of *VEGF* expression in cultured EC of mice subjected to MS or CT for 24 h. *GAPGH* was used as loading controls. Representative photographs are shown. Data are shown as folds of Sham or CT in WT mice and expressed as mean ± S.E.M. of five experiments (n = 5). * $p<0.05$ *vs* Sham or CT; # $p<0.05$ *vs* WT with TAC or MS. (E) Coronary perfusion pressure in perfused mouse heart. The hearts of WT, TG and KO mice subjected to TAC or sham for 4 weeks were excised and subjected to a nonrecirculating Langendorff mode. Coronary perfusion pressure was measured by 3 times for each heart during perfusion of 30 min. Values are expressed as mean ± S.E.M. of three hearts (n = 3). * $p<0.05$ *vs* similar genotype sham mice; # $p<0.05$ *vs* WT with TAC.

3.5. Effects of HIF-1 and p53 on HSF1-regulated in vitro formation of vasculatures after MS

We finally examined the *in vitro* effects of HIF-1 and p53 on the formation of microvessels using cultured EC. The abilities to form tube-like structures were not different between the TG- and the KO-EC without MS (Figs. 5A–D). After MS, the microvascular tubes were less formed by the KO-EC (Figs. 5A, C) but more formed by the TG-EC (Figs. 5B, D) than the EC without MS. Transfection of a *HIF-1* gene into the KO-EC did not make them to form more vasculatures, whereas a siRNA of *p53* gene did enhance the tube-formation by the KO-EC after MS (Figs. 5A, C). Also, transfection of a *p53* gene into the TG-EC did not affect the ability of the EC to form more vasculatures after MS, a siRNA of *HIF-1* gene impaired the ability of the cells (Figs. 5B, D). We also examined the expression of HIF1 and p53 proteins in nucleus of these cells. *HIF-1* gene transfection did not increase the HIF-1 nor suppress the p53 proteins in nucleus of the KO-EC after MS, while inhibition of *p53* by a siRNA induced a downregulation of p53 protein with an elevation of HIF-1 protein in the nucleus of the same cell model (Fig. 5E). In the TG-EC, which showed a high level of HIF-1 protein and a low p53 protein in the nucleus after MS, however, *p53* gene transfection could not

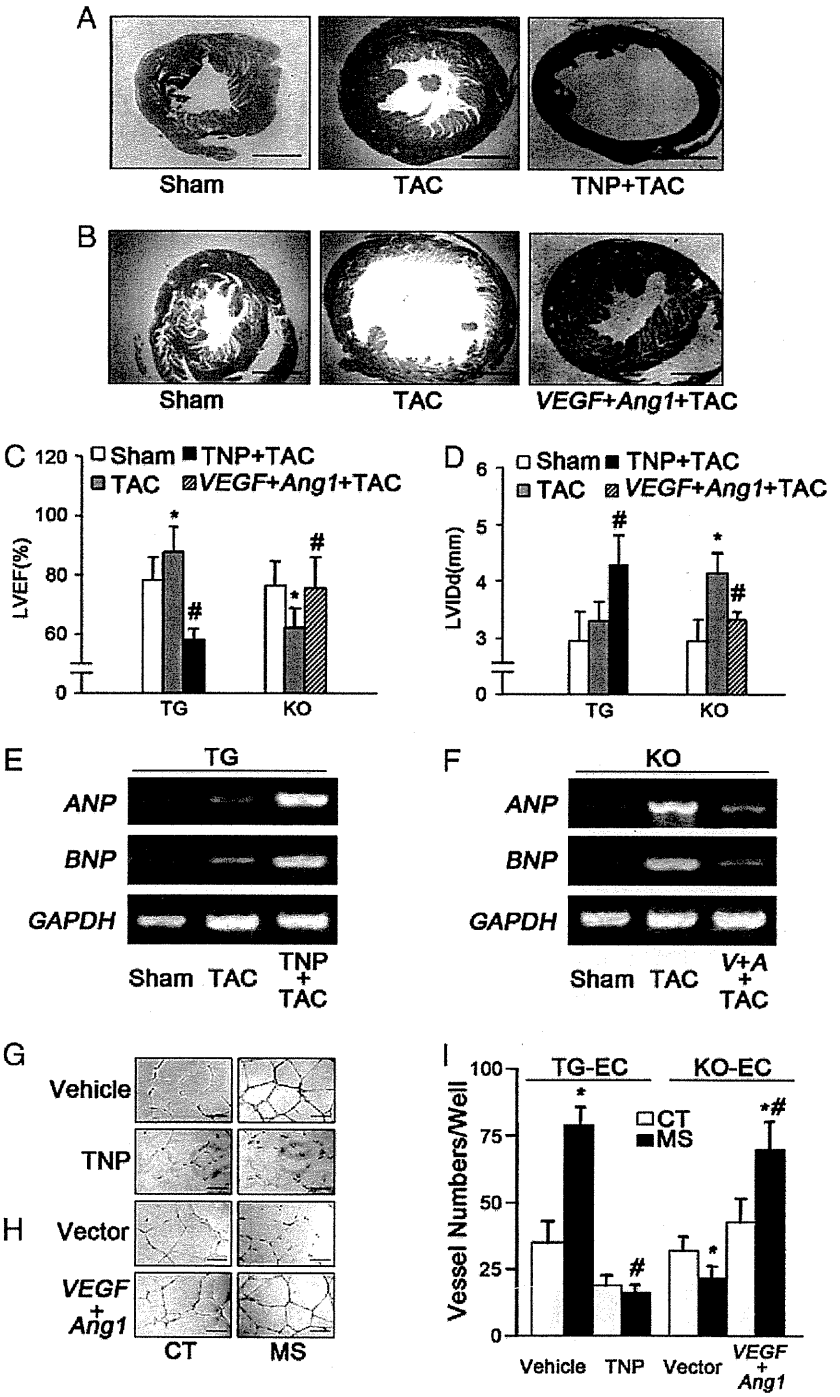

Fig. 2. Effects of angiogenesis on HSF1-related cardiac hypertrophy. (A) Inhibition of cardiac hypertrophy by TNP-470 in *HSF1* TG mice. TG mice were treated with TNP-470 (TNP, 30 mg/kg/day) or vehicle, and subjected to TAC or sham for 4 weeks. (B) Effects of overexpression of *VEGF* with *Ang-1* in myocardium of *HSF1* KO mice. Adenovirus vectors encoding *VEGF* and *Ang-1* genes were injected into myocardium of KO mice before TAC. Heart sections were stained with H–E (scale bars: 1 mm). TNP-TAC, TNP-470-treated mice with TAC; *VEGF*+*Ang-1*-TAC, *VEGF* and *Ang-1* gene-injected mice with TAC. (C and D) LVEF and LVIDd analyzed by echocardiography. Data are expressed as mean ± S.E.M. of five mice (n = 5). * $p<0.05$ *vs* Sham; # $p<0.05$ *vs* TAC. (E and F) RT-PCR analyses for *ANP* and *BNP* expression in the heart of mice. *GAPGH* was used as loading controls. Representative photographs from 3 independent experiments are shown. (G and H) Effects of TNP-470 and *VEGF/Ang-1* gene transfection on formation of vasculatures. EC were isolated from LV of the TG (G) and KO (H) mice. Cultured EC were added by TNP-470 (TNP, 10^{-5} mol/L) or vehicle (G) or transfected with *VEGF* and *Ang-1* genes or empty vector (H). Representative photographs of vessel-like tubes are shown (scale bar: 20 μm). CT, control; MS, mechanical stretch. (I) Quantitative analyses for vessel formation. Total vessels were counted in whole dish. Data are expressed as mean ± S.E.M. of five independent experiments (n = 5). * $p<0.05$ *vs* CT; # $p<0.05$ *vs* vehicle or vector treated EC with MS.

increase the p53 protein nor did decrease the HIF-1 protein, while a siRNA of *HIF-1* might attenuate the HIF-1 protein in the nucleus after MS (Fig. 5F). These results collectively suggest that HSF1-dependent microvascular formation by EC is mediated by p53-regulated HIF-1 protein.

4. Discussion

Here, we demonstrate a novel mechanism by which HSF1 protects the heart against chronic pressure overload. HSF1 preserves cardiac adaptation, at least in part, through promoting cardiac EC-dependent

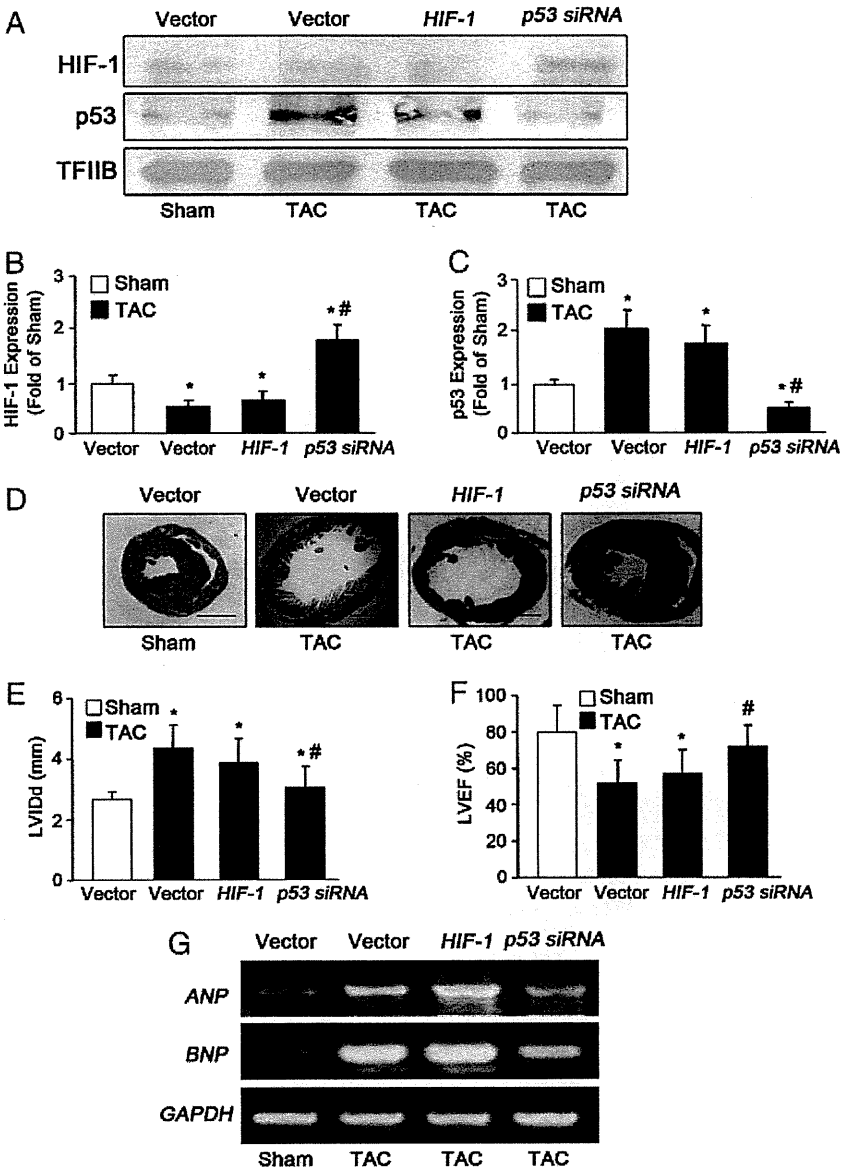

Fig. 3. Effects of *HIF-1* gene and siRNA of *p53* on cardiac hypertrophy in *HSF1* KO mice. Adenoviral vectors encoding *HIF-1* and siRNA *of p53* or empty vectors (Vector) were injected into the hearts of *HSF1* KO mice, and the mice were subjected to TAC or sham for 4 weeks. (A) Expression of HIF-1 and p53 proteins. Nuclear proteins were extracted from LV tissues and subjected to a Western blot analysis using anti HIF-1α and p53 antibodies. TFIIB expression was used as loading controls. Representative photographs are shown. (B and C) Expressions of HIF-1 and p53 proteins were quantified as folds of TFIIB expression in Sham. Data are expressed as mean ± S.E.M. of five independent experiments (n = 5). * $p<0.05$ *vs* Sham; # $p<0.05$ *vs* TAC mice with vector transfection. (D–F) Echocardiography and H–E staining were used to evaluate cardiac hypertrophy and functions. Representative H–E stained sections are shown (D) (scale bars: 1 mm). LVIDd (E) and LVEF (F) were expressed as mean ± S.E.M. of five mice. * $p<0.05$ *vs* Sham; # $p<0.05$ *vs* TAC mice with vector injection. (G) RT-PCR analyses for *ANP* and *BNP* expression in the heart of mice. *GAPGH* was used as loading controls. Representative photographs from 3 independent experiments are shown.

angiogenesis, which is relative to suppression of p53 and subsequent upregulation of HIF-1 during chronic pressure overload.

Physiological cardiac hypertrophy by exercise is adaptive and has better prognosis than pressure overload-induced cardiac hypertrophy. Upregulation of HSF1 and HSPs account, at least in part, for adaptive responses of the heart to exercise [6]. Although pressure overload-induced cardiac hypertrophy usually develops to heart failure eventually, exercise-induced cardiac hypertrophy does not [4,5]. Interestingly, HSF1 and HSPs can be upregulated for a long period by exercise but not by chronic pressure overload [6]. Although the mechanism by which HSF1 is upregulated after exercise remains unknown, these data strongly suggest that maintaining of HSF1 at a higher level could preserve adaptation of the heart in response to a chronic pressure overload. In the present study, under sustained pressure overload, overexpression of the HSF1 in mice heart increased expression of HSP70, enhanced cardiac hypertrophy and delayed cardiac dysfunctions, while decrease of HSF1 impaired adaptive cardiac hypertrophy and aggravated cardiac dysfunctions, consistent with our previous report [6].

It has been speculated that HSF1/HSPs-associated protection of the heart is due to a protection of cardiomyocytes from death [6,21,24,25], which is mediated by antagonizing the proinflammatory pathways [6]. We recently observed that inhibition of angiogenesis causes transition of an adaptive hypertrophy to cardiac dysfunctions during chronic pressure overload and that increases in cardiomyocyte death evaluated by a TUNEL method were observed from 2 weeks but not at early phase after pressure overload [10]. In our present results,

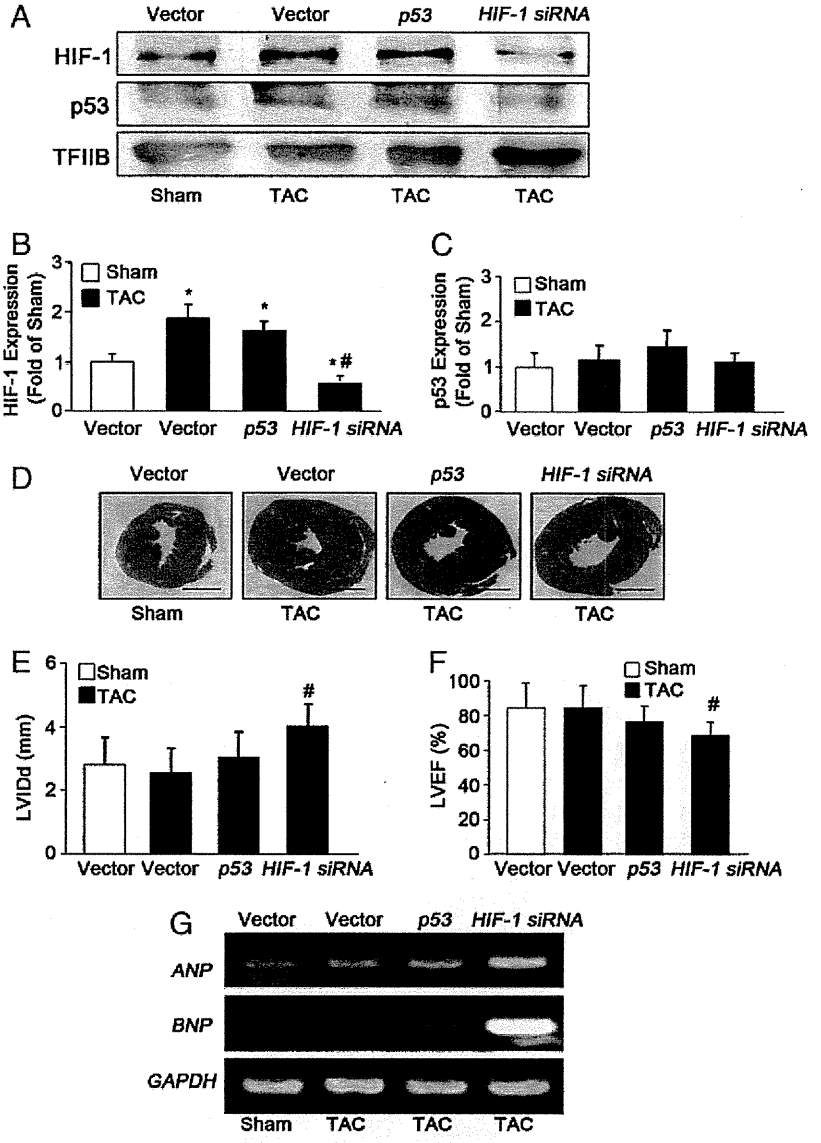

Fig. 4. Effects of *p53* gene and siRNA of *HIF-1* on cardiac hypertrophy in *HSF1* TG mice. Adenoviral vectors encoding *p53* gene and siRNA of *HIF-1* or empty vectors (Vector) were injected into hearts of the *HSF1* TG mice, and the mice were subjected to TAC or sham for 4 weeks. (A) Expression of HIF-1 and p53 proteins. Nuclear proteins were extracted from LV tissues and subjected to a Western blot analysis using anti HIF-1α and p53 antibodies. TFIIB expression was used as loading controls. Representative photographs are shown. (B and C) Expressions of HIF-1 and p53 proteins were quantified as folds of TFIIB expression in Sham. Data are expressed as mean ± S.E.M. of five independent experiments (n = 5). * $p<0.05$ *vs* Sham; # $p<0.05$ *vs* TAC mice with vector transfection. (D–F) Echocardiography and H–E staining were used to evaluate cardiac hypertrophy and functions. Representative H–E staining is shown (D) (scale bars: 1 mm). LVIDd (E) and LVEF (F) were expressed as mean ± S.E.M. of five mice (n = 5). * $p<0.05$ *vs* Sham; # $p<0.05$ *vs* TAC mice with vector injection. (G) RT-PCR analyses for *ANP* and *BNP* expression in the heart of mice. *GAPGH* was used as loading controls. Representative photographs from 3 independent experiments are shown.

vasculatures was significantly more formed and *VEGF* was more expressed in hearts of *HSF1* TG mice, whereas vascular formation and *VEGF* expression were both less in the heart of *HSF1* KO mice compared to WT mice after TAC. Especially, inhibition of angiogenesis abolished preservation of cardiac adaptation in *HSF1* TG mice, while promoting angiogenesis in the heart of *HSF1* KO mice improved the maladaptive hypertrophy in response to chronic pressure overload. These results collectively show a pivotal role of angiogenesis in addition to cardiomyocyte survival in the effect of HSF1 on a work-loaded heart. HSF1 usually induces HSPs expression including HSP70 [6]. Our data also confirm that HSP70 is regulated by HSF1. It has been reported that knockdown of HSP70 inhibited angiogenesis induced by VEGF [26]. However, we observed that overexpression of VEGF did not change the expression of HSP70 in HSF1 KO mice, and knockdown of HSP70 did not abolish the protective effects of VEGF on the work-loaded hearts in wild type mice. Although the reason for this distinction is unknown, HSP70 is regulated by HSF1 but not by VEGF in the setting of our present study.

HIF-1, a key transcription factor for the hypoxic induction of angiogenesis factors, can induce adaptive metabolic change as well as VEGF-mediated angiogenesis, which lead to the formation of new vessels [27,28]. In previous studies, upregulation of HIF-1 expression and activation has been indicated to be important not only for cardioprotection against hypoxia during myocardial ischemia/reperfusion and by post-conditioning [29] but also for the adaptive mechanism of cardiac hypertrophy at early phase during pressure overload [10]. In the present study, expression of *HIF-1* was high in the TG heart but low in the KO heart after TAC, suggesting that HSF1 may regulate expression of *HIF-1*. Inhibition of HIF-1 by a siRNA significantly suppressed adaptive cardiac hypertrophy in *HSF1* TG mice, suggesting that HIF-1 plays a role in the effect of HSF1/HSP70. However, transfection of *HIF-1* gene in the heart lacking HSF1, which

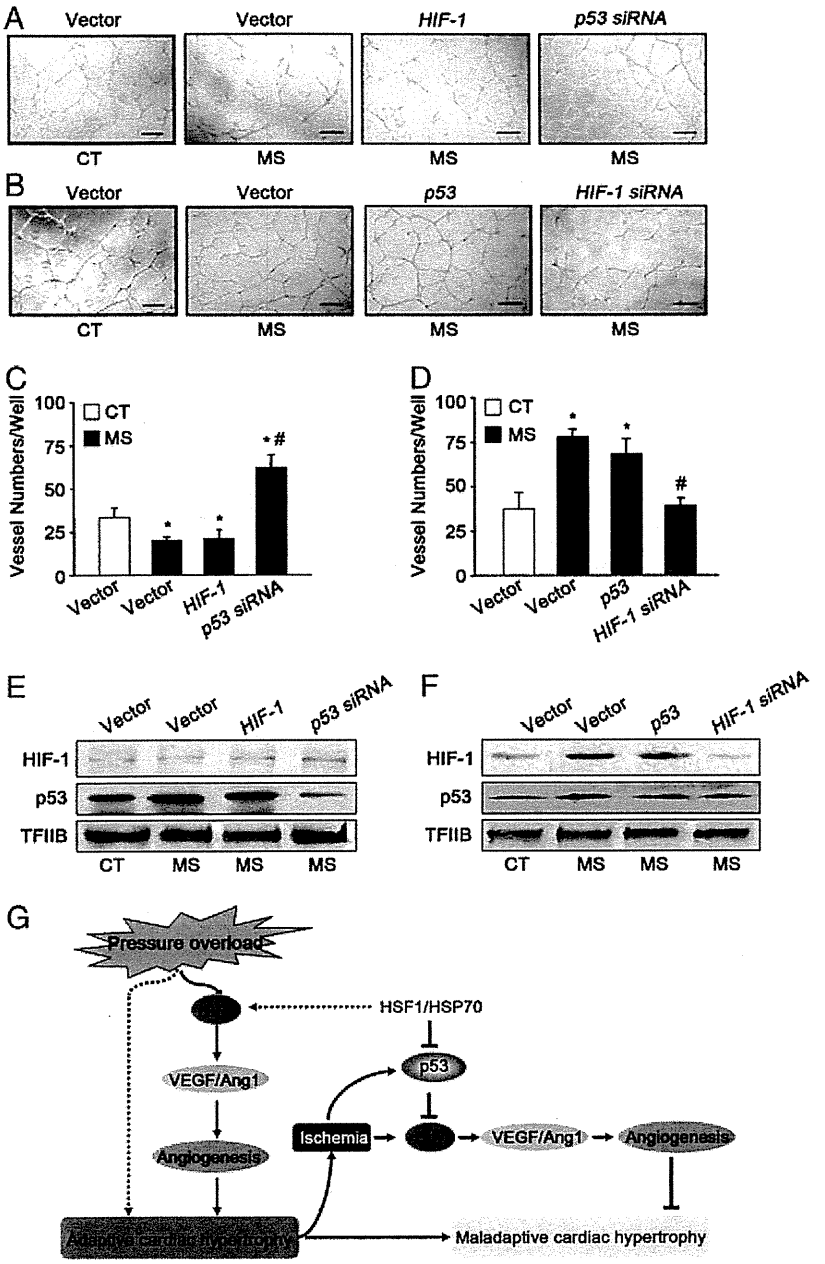

Fig. 5. Effects of *HIF-1*, *p53* and their siRNA on microvascular formation. EC isolated from the LV of KO and TG mice were transfected with *HIF-1*, *p53* genes, their siRNA or empty vectors for 24 h before subjected to vascular formation experiments, respectively. (A and B) Representative photographs of vasculatures formed by the KO-EC (A) and the TG-EC (B) are shown (scale bar: 50 μm). CT, control; MS, mechanical stretch. (C and D) Quantitative analysis. Total tube-like structures formed by the KO-EC (C) and the TG-EC (D) were counted in whole dish. Data are expressed as mean ± S.E.M. of five independent experiments (n = 5). * $p<0.05$ *vs* CT; # $p<0.05$ *vs* vector transfected EC with MS stimulation. (E and F) Expressions of HIF-1 and p53 proteins. Nuclear proteins were extracted from the KO-EC (E) and TG-EC (F) transfected with *HIF-1*, *p53*, their siRNA or empty vectors for 24 h and stimulated with MS or CT for 24 h, and subjected to a Western blot analysis using anti HIF-1α and p53 antibodies. TFIIB expression was used as loading controls. Representative blots from five independent experiments are shown. (G) Proposed mechanism underlying the effects of HSF1/HSP70 on pressure overload-induced cardiac hypertrophy.

could not induce elevation of HIF-1 protein in nuclear, did not benefit the maladaptive hypertrophy after TAC although overexpression of its downstream factors *Ang-1* and *VEGF* did improve cardiac dysfunctions in the same type of mice, indicating that there might be another mechanism existing in the *HSF1* KO heart to directly suppress the effect of HIF-1 but not of its downstream factors during pressure overload. It has been reported that HSF1 can act as a modifier of tumorigenesis through regulation of p53, which is required for tumor initiation and maintenance in a variety of cancer models [30]. We also found that p53 plays a critical role in the inhibition of adaptive upregulation of HIF-1 during a chronic pressure overload [10], which induces transition of cardiac hypertrophy to dysfunctions. In the present study, expression of *p53* was significantly downregulated in the myocardium of *HSF1* TG mice but upregulated in the KO heart after TAC, and injecting a *p53* gene into the *HSF1* TG heart could not induce an elevation of p53 protein, suggesting that HSF1/HSP70 negatively regulates p53 expression. Transfection of a siRNA into myocardium to knockdown the expression of p53, which induced an elevation of HIF-1 protein, significantly reversed the maladaptive hypertrophy in *HSF1* KO mice, suggesting that p53 is a suppressor of HIF-1 in the HSF1 lacking heart. These results collectively indicate that HSF1/HSP70 exerts effects on the cardiac adaptation during pressure

overload through suppression of p53 expression and subsequent upregulation of HIF-1 expression.

Since angiogenesis is regulated by EC and hypertrophic responses of cardiac myocytes after mechanical stretch were similar among *HSF1* TG, KO and WT cardiomyocytes, we hypothesized that HIF-1 and p53 contribute to HSF1-regulated cardiac adaptation through cardiac EC. Expression of *HIF-1* was high in the EC of TG heart but low in the EC of KO heart while expression of *p53* was low in the EC of TG mice but high in the EC of KO heart after mechanical stretch. Furthermore, knockdown of p53 protein by a siRNA, which induced an elevation of HIF-1 protein in nucleus, rather than transfection of a *HIF-1* gene, which could not increase the HIF-1 protein, significantly improved the vascular forming abilities of the KO-EC, and downregulation of HIF-1 protein by a siRNA of *HIF-1* but not transfection of a *p53* gene, which could not induce a elevation of p53 protein in nucleus, did impair the formation of vasculatures by the TG-EC. These *in vitro* results are consistent with the *in vivo* experiments.

In the present study, introduction of the HIF-1-gene did not significantly alter the *HIF-1* expression in myocardium of HSF1 KO mice nor did transfection of the *p53* gene alter the p53 protein expression in myocardium of HSF1 TG mice with TAC. In sham operated *HSF1* KO and TG mice, however, we observed that the similar transfection induced significant increases in HIF-1 or p53 protein expression, respectively (data not shown). Although the exact mechanisms for these results are not clearly understood at present, we speculate two possibilities. Firstly, in *HSF1* KO mice, p53 expression was at a very high level due to the deficiency of the HSF1 and HSPs, and was activated by pressure overload. The activated p53 could therefore inhibit the increase in the expression of the transfected HIF-1. Secondly, in *HSF1* TG mice, overexpressed HSF1 and HSPs were activated by pressure overload, thereby abrogating the elevation of the transfected p53 expression.

Although the direct effects of angiogenesis induced by angiogenetic factors on cardiac hypertrophy and performance need to be further investigated, our present study collectively indicates that HSF1/HSPs-dependent long-term maintenance of adaptive cardiac hypertrophy during pressure overload is, at least in part, due to the increase or maintenance of formation of functional vasculatures by EC, which is regulated by the suppression of p53 and subsequent increase in HIF-1 transcriptional activity (Fig. 5G). These results also suggest a proper target cell for the treatment of heart failure.

Supplementary materials related to this article can be found online at doi:10.1016/j.yjmcc.2011.07.030.

Disclosures

None.

Acknowledgments

This work was supported by the National Science Fund for Distinguished Young Scholars from the Natural Science Foundation of China (30525018), National Basic Research Program of China (2007CB512003), China Doctoral Foundation (20060246079) and National Natural Science Fund of China (30971250) to Y. Zou and National Natural Science Fund of China (30871073) to H. Jiang.

References

[1] Levy D, Garrison RJ, Savage DD, Kannel WB, Castelli WP. Prognostic implications of echocardiographically determined left ventricular mass in the Framingham Heart Study. N Engl J Med 1990;322:1561–6.
[2] Frey N, Olson EN. Cardiac hypertrophy: the good, the bad, and the ugly. Annu Rev Physiol 2003;65:45–79.
[3] Katz AM. Cardiomyopathy of overload. A major determinant of prognosis in congestive heart failure. N Engl J Med 1990;322:100–10.
[4] Adams TD, Yanowitz FG, Fisher AG, Ridges JD, Lovell K, Pryor TA. Noninvasive evaluation of exercise training in college-age men. Circulation 1981;64:958–65.
[5] Pelliccia A, Maron BJ. Outer limits of the athlete's heart, the effect of gender, and relevance to the differential diagnosis with primary cardiac diseases. Cardiol Clin 1997;15:381–96.
[6] Sakamoto M, Minamino T, Toko H, Kayama Y, Zou Y, Sano M, et al. Upregulation of heat shock transcription factor 1 plays a critical role in adaptive cardiac hypertrophy. Circ Res 2006;99:1411–8.
[7] Staib JL, Quindry JC, French JP, Criswell DS, Powers SK. Increased temperature, not cardiac load, activates heat shock transcription factor 1 and heat shock protein 72 expression in the heart. Am J Physiol Regul Integr Comp Physiol 2007;292:R432–9.
[8] Nishizawa J, Nakai A, Komeda M, Ban T, Nagata K. Increased preload directly induces the activation of heat shock transcription factor 1 in the left ventricular overloaded heart. Cardiovasc Res 2002;55:341–8.
[9] Chang J, Wasser JS, Cornelussen RNM, Knowlton AA. Activation of heat-shock factor by stretch-activated channels in rat hearts. Circulation 2001;104:209–14.
[10] Sano M, Minamino T, Toko H, Miyauchi H, Orimo M, Qin Y, et al. p53-induced inhibition of HIF-1 causes cardiac dysfunction during pressure overload. Nature 2007;446:444–8.
[11] Kang MJ, Jung SM, Kim MJ, Bae JH, Kim HB, Kim JY, et al. DNA-dependent protein kinase is involved in heat shock protein-mediated accumulation of hypoxia-inducible factor-1α in hypoxic preconditioned HepG2 cells. FEBS J 2008;275:5969–81.
[12] Baird NA, Turnbull DW, Johnson EA. Induction of the heat shock pathway during hypoxia requires regulation of heat shock factor by hypoxia-inducible factor-1. J Biol Chem 2006;281:38675–81.
[13] Zylicz M, King FW, Wawrzynow A. Hsp70 interactions with the p53 tumour suppressor protein. EMBO J 2001;20:4634–8.
[14] King FW, Wawrzynow A, Hohfeld J, Zylicz M. Co-chaperones Bag-1, Hop and Hsp40 regulate Hsc70 and Hsp90 interactions with wild-type or mutant p53. EMBO J 2001;20:6297–305.
[15] Walerych D, Kudla G, Gutkowska M, Wawrzynow B, Muller L, King FW, et al. Hsp90 chaperones wild-type p53 tumor suppressor protein. J Biol Chem 2004;279:48836–45.
[16] Nakai A, Suzuki M, Tanabe M. Arrest of spermatogenesis in mice expressing an active heat shock transcription factor 1. EMBO J 2000;19:1545–54.
[17] Inouye S, Izu H, Takaki E, Suzuki H, Shirai M, Yokota Y, et al. Impaired IgG production in mice deficient for heat shock transcription factor 1. J Biol Chem 2004;279:38701–9.
[18] Sangaralingham SJ, Tse MY, Pang SC. Estrogen protects against the development of salt-induced cardiac hypertrophy in heterozygous proANP gene-disrupted mice. J Endocrinol 2007;194:143–52.
[19] Pedram A, Razandi M, Lubahn D, Liu J, Vannan M, Levin ER. Estrogen inhibits cardiac hypertrophy: role of estrogen receptor-beta to inhibit calcineurin. Endocrinology 2008;149:3361–9.
[20] Zou Y, Akazawa H, Qin Y, Sano M, Takano H, Minamino T, et al. Mechanical stress activates angiotensin II type 1 receptor without the involvement of angiotensin II. Nat Cell Biol 2004;6:499–506.
[21] Xu W, Yu Z, Xie Y, Huang G, Shu X, Zhu Y, et al. Therapeutic effect of intermittent hypobaric hypoxia on myocardial infarction in rats. Basic Res Cardiol 2011;106:329–42.
[22] Chorianopoulos E, Heger T, Lutz M, Frank D, Bea F, Katus HA, et al. FGF-inducible 14-kDa protein (Fn14) is regulated via the RhoA/ROCK kinase pathway in cardiomyocytes and mediates nuclear factor-kappaB activation by TWEAK. Basic Res Cardiol 2010;105:301–13.
[23] Yamazaki T, Komuro I, Kudoh S, Zou Y, Shiojima I, Mizuno T, et al. Mechanical stress activates protein kinase cascade of phosphorylation in neonatal rat cardiac myocytes. J Clin Invest 1995;96:438–46.
[24] Zou Y, Zhu W, Sakamoto M, Qin Y, Akazawa H, Toko H, et al. Heat shock transcription factor 1 protects cardiomyocytes from ischemia/reperfusion injury. Circulation 2003;108:3024–30.
[25] Yan LJ, Christians ES, Liu L, Xiao X, Sohal RS, Benjamin IJ. Mouse heat shock transcription factor 1 deficiency alters cardiac redox homeostasis and increases mitochondrial oxidative damage. EMBO J 2003;21:5164–72.
[26] Shiota M, Kusakabe H, Izumi Y, Hikita Y, Nakao T, Funae Y, et al. Heat shock cognate protein 70 is essential for Akt signaling in endothelial function. Arterioscler Thromb Vasc Biol 2010;30:491–7.
[27] Semenza GL. Targeting HIF-1 for cancer therapy. Nat Rev Cancer 2003;3:721–32.
[28] Pugh CW, Ratcliffe PJ. Regulation of angiogenesis by hypoxia: role of the HIF system. Nat Med 2003;9:677–84.
[29] Zhao H, Wang X, Wang Y, Wu Y, Li X, Lv X, et al. Attenuation of myocardial injury by postconditioning: role of hypoxia inducible factor-1α. Basic Res Cardiol 2010;105:109–18.
[30] Dai C, Whitesell L, Rogers AB, Lindquist S. Heat shock factor 1 is a powerful multifaceted modifier of carcinogenesis. Cell 2007;130:1005–18.

Global Mapping of Cell Type–Specific Open Chromatin by FAIRE-seq Reveals the Regulatory Role of the NFI Family in Adipocyte Differentiation

Hironori Waki[1,2☯], Masahiro Nakamura[1☯], Toshimasa Yamauchi[1☯*], Ken-ichi Wakabayashi[3☯], Jing Yu[1], Lisa Hirose-Yotsuya[1], Kazumi Take[1], Wei Sun[1], Masato Iwabu[1,4], Miki Okada-Iwabu[1,5], Takanori Fujita[3], Tomohisa Aoyama[1], Shuichi Tsutsumi[3], Kohjiro Ueki[1], Tatsuhiko Kodama[6], Juro Sakai[7*], Hiroyuki Aburatani[3*], Takashi Kadowaki[1*]

1 Department of Diabetes and Metabolic Diseases, Graduate School of Medicine, University of Tokyo, Tokyo, Japan, **2** Functional Regulation of Adipocytes, Graduate School of Medicine, University of Tokyo, Tokyo, Japan, **3** Genome Science Division, Laboratory of Systems Biology and Medicine, Research Center for Advanced Science and Technology, University of Tokyo, Tokyo, Japan, **4** Department of Integrated Molecular Science on Metabolic Diseases, 22nd Century Medical and Research Center, University of Tokyo, Tokyo, Japan, **5** Molecular Medicinal Sciences on Metabolic Regulation, Graduate School of Medicine, University of Tokyo, Tokyo, Japan, **6** Systems Biology and Medicine Division, Laboratory of Systems Biology and Medicine, Research Center for Advanced Science and Technology, University of Tokyo, Tokyo, Japan, **7** Metabolic Medicine Division, Laboratory of Systems Biology and Medicine, Research Center for Advanced Science and Technology, University of Tokyo, Tokyo, Japan

Abstract

Identification of regulatory elements within the genome is crucial for understanding the mechanisms that govern cell type–specific gene expression. We generated genome-wide maps of open chromatin sites in 3T3-L1 adipocytes (on day 0 and day 8 of differentiation) and NIH-3T3 fibroblasts using formaldehyde-assisted isolation of regulatory elements coupled with high-throughput sequencing (FAIRE-seq). FAIRE peaks at the promoter were associated with active transcription and histone modifications of H3K4me3 and H3K27ac. Non-promoter FAIRE peaks were characterized by H3K4me1+/me3-, the signature of enhancers, and were largely located in distal regions. The non-promoter FAIRE peaks showed dynamic change during differentiation, while the promoter FAIRE peaks were relatively constant. Functionally, the adipocyte- and preadipocyte-specific non-promoter FAIRE peaks were, respectively, associated with genes up-regulated and down-regulated by differentiation. Genes highly up-regulated during differentiation were associated with multiple clustered adipocyte-specific FAIRE peaks. Among the adipocyte-specific FAIRE peaks, 45.3% and 11.7% overlapped binding sites for, respectively, PPARγ and C/EBPα, the master regulators of adipocyte differentiation. Computational motif analyses of the adipocyte-specific FAIRE peaks revealed enrichment of a binding motif for nuclear family I (NFI) transcription factors. Indeed, ChIP assay showed that NFI occupy the adipocyte-specific FAIRE peaks and/or the PPARγ binding sites near PPARγ, C/EBPα, and aP2 genes. Overexpression of NFIA in 3T3-L1 cells resulted in robust induction of these genes and lipid droplet formation without differentiation stimulus. Overexpression of dominant-negative NFIA or siRNA-mediated knockdown of NFIA or NFIB significantly suppressed both induction of genes and lipid accumulation during differentiation, suggesting a physiological function of these factors in the adipogenic program. Together, our study demonstrates the utility of FAIRE-seq in providing a global view of cell type–specific regulatory elements in the genome and in identifying transcriptional regulators of adipocyte differentiation.

Citation: Waki H, Nakamura M, Yamauchi T, Wakabayashi K-i, Yu J, et al. (2011) Global Mapping of Cell Type–Specific Open Chromatin by FAIRE-seq Reveals the Regulatory Role of the NFI Family in Adipocyte Differentiation. PLoS Genet 7(10): e1002311. doi:10.1371/journal.pgen.1002311

Editor: Jason D. Lieb, The University of North Carolina at Chapel Hill, United States of America

Received April 17, 2011; **Accepted** August 9, 2011; **Published** October 20, 2011

Funding: This work was supported by a Grant-in-Aid for Young Scientists (B) from the Japan Society for the Promotion of Science (JSPS) (#20890055, #21790864, H Waki, http://www.jsps.go.jp/english/), funds from the Kanae Foundation for the Promotion of Medical Science (H Waki, http://kanae.sanofi-aventis.co.jp/en/index.html), Senri Life Science Foundation (H Waki, http://www.senri-life.or.jp/), Takeda Science Foundation (H Waki, http://www.takeda-sci.or.jp/), Japan Foundation for Applied Enzymology (H Waki, http://www.mt-pharma.co.jp/jfae/index.html), Sankyo Foundation of Life Science (H Waki, http://www.sankyo-fdn.or.jp/), Banyu Life Science Foundation International (H Waki, http://www.banyu-zaidan.or.jp/index.html), and by a Grants-in-Aid for Scientific Research (S) from the Ministry of Education, Culture, Sports, Science, and Technology (#20221009, H Aburatani, http://www.jsps.go.jp/english/), and Grant-in-Aid for Scientific Research on Innovative Areas (Research in a proposed research area) "Molecular Basis and Disorders of Control of Appetite and Fat Accumulation (to T Yamauchi), Funding Program for Next Generation World-Leading Researchers (NEXT Program) (to T Yamauchi). These institutions had no role in study design, data collection and analysis, decision to publish, or preparation of the manuscript.

Competing Interests: The authors have declared that no competing interests exist.

* E-mail: kadowaki-3im@h.u-tokyo.ac.jp (T Kadowaki); haburata-tky@umin.ac.jp (H Aburatani); jmsakai-tky@umin.ac.jp (J Sakai); tyamau-tky@umin.net (T Yamauchi)

☯ These authors contributed equally to this work.

Introduction

Sequencing allowed identification and mapping of the human genome [1]. Transcriptional regulation of genes is essential for manifesting cellular phenotypes and complex biological processes. Coordinated actions of transcription factors and cofactors on regulatory DNA sequences produce transcriptional activation of the eukaryotic gene. Therefore, identification and mapping of the genome's regulatory elements is critical for understanding how cell-type-selective regulation of genes in the genome is achieved.

Author Summary

Humans consist of a few hundred types of specialized-function cells. Spatial and temporal transcriptional regulation of genes is essential for manifestation of cellular phenotypes. Identification of regulatory regions in the genome is central to understanding the mechanism of cell type–specific gene regulation. Recently developed high-throughput sequencing technology and computational analyses allow genome-wide investigation of the genome's chromatin structure. Using the FAIRE-seq technique, we identified the genome's open chromatin regions, which harbor regulatory elements in adipocytes. Open chromatin regions distal to genes' transcription start sites significantly differ among cell types. Multiple cell type–specific open chromatin regions exist near genes regulated during adipocyte differentiation. Computational motif analysis of adipocyte-specific open chromatin regions revealed enrichment of a binding motif for the NFI transcription factor family. These factors bind to the regulatory elements near adipogenic PPARγ, C/EBPα, and aP2 genes and regulate their expression. Overexpression of NFIA in 3T3-L1 cells resulted in robust induction of these genes and lipid droplet formation without differentiation stimulus and knockdown of NFIA or NFIB significantly suppressed both induction of genes and lipid accumulation during differentiation. Our study demonstrates the utility of FAIRE-seq in providing a global view of regulatory elements and in identifying transcriptional regulators of cellular functions.

Traditionally, regulatory elements have been identified by DNase I hypersensitivity assay combined with Southern blot analysis [2]. That assay coupled with microarray or high-throughput sequencing (DNase-Chip or DNase-seq) were effectively applied in genome-wide identification of open chromatin regions [3,4,5,6]. Lieb and his colleagues recently developed formaldehyde-assisted isolation of regulatory elements (FAIRE) as a simple procedure to isolate nucleosome-depleted DNA from chromatin [7,8]. FAIRE detects open chromatin structure much the way the DNase I hypersensitivity assay does [8,9]—but with advantages, like obviating the need for clean nuclei preparation and laborious enzyme titrations [7,8]. Coupled with high-throughput sequencing (FAIRE-seq), FAIRE allows unbiased identification of potential regulatory elements without requiring prior knowledge of (or about) binding factors. FAIRE-seq's genome-wide detection of open chromatin genomic regions in human pancreatic islets was successfully used to determine a causal single nucleotide polymorphism in loci associated with type 2 diabetes development in genome-wide association studies [10].

The adipocyte is central in controlling energy balance and whole-body glucose and lipid homeostasis [11]. Advances in adipocyte research have shown that adipose tissue stores excess energy *and* secretes hormones and metabolites to communicate with other organs, maintaining systemic metabolic homeostasis [12]. Peroxisome proliferator-activated receptor gamma (PPARγ; NR1C3) is both necessary [13,14,15] and sufficient [16] for adipocyte differentiation. Necessary for both development and maintenance of mature adipocytes, PPARγ is crucial in systemic glucose and lipid homeostasis [13,14,15,17], and, importantly, is the molecular target of thiazolidinediones, widely prescribed for obese diabetics [18]. C/EBPα-β-δ act with PPARγ, forming the adipogenic transcription cascade [19]. C/EBPβ and δ are induced by adipogenic stimulus, inducing PPARγ, which activates expression of C/EBPα, which binds and further activates expression of PPARγ, providing a positive regulatory loop [11,20]. Genome-wide approaches now dissect the transcriptional mechanisms of adipocyte differentiation. ChIP-chip or ChIP-seq studies of adipogenic regulators [21,22,23,24,25,26,27,28,29] have provided valuable mechanistic insights into adipogenic transcription never before gained by conventional experiments: New concepts include co-localization of PPARγ and cell type–specific transcription factors [27], low conservation rate of PPARγ binding sites between murine and human adipocytes [28] and the role of C/EBPβ as a pioneer factor that establishes "hot spots" where multiple adipogenic regulators cooperatively work in the very early stage of differentiation [6].

Our study took an unbiased approach to mapping adipocyte-specific regulatory elements in the genome by using FAIRE in 3T3-L1 adipocytes (on day 0 and day 8 of differentiation) and NIH-3T3 fibroblasts. We show that the FAIRE peaks contain regulatory elements such as promoters, enhancers and insulators, and that adipocyte-specific non-promoter FAIRE peaks are functionally linked to genes regulated during differentiation—about half these peaks being overlapped by PPARγ. We show that highly regulated genes in adipocyte differentiation are associated with clusters of multiple adipocyte-specific non-promoter FAIRE peaks. Furthermore, because FAIRE does not require a prioi knowledge of bound transcription factors, we could employ computational motif analyses of DNA sequences from the adipocyte-specific FAIRE peaks in an unbiased manner and identify a motif for nuclear family I (NFI) transcription factors in addition to motifs for PPAR and C/EBPs. We show the functional role of NFIA and NFIB in adipocyte differentiation. We demonstrate the utility of FAIRE-seq both in providing a global view of cell type–specific *cis*-regulatory elements in the genome and identifying transcriptional regulators of adipocyte differentiation.

Results

Genome-Wide Profiling of Open Chromatin Regions in 3T3-L1 Adipocytes by FAIRE-seq

Regulatory elements in the genome are characterized by open chromatin structures accessible to regulatory factors [30]. To explore genome-wide changes in open chromatin conformation during adipocyte differentiation, we used FAIRE—a method of isolating genomic regions depleted of nucleosomes [7]—combined with high-throughput sequencing (FAIRE-seq) to identify open chromatin sites in the adipogenic cell line 3T3-L1 before (day 0) and after (day 8) differentiation and in NIH-3T3 fibroblasts, which cannot differentiate into adipocytes. This approach identified in the genome 37,781 FAIRE peaks in 3T3-L1 on day 0 and 26,611 on day 8, plus 36,111 in NIH-3T3 cells—all, with a false discovery rate of $<10^{-4}$. By using ChIP-seq analyses, we also generated genome-wide maps of binding sites for PPARγ, the master regulator of adipocyte differentiation, for RXRα, its heterodimer partner, for histone H3 lysine 4 trimethylation (H3K4me3), and for CCCTC-binding factor (CTCF) [31].

Figure 1 shows a representative map of results generated near *Klf15* and *Pparg*, both transcription factors up-regulated by differentiation, and both important in adipocyte differentiation [16,32]. Consistent with previous observations [10], 28% of the FAIRE peaks were detected near the transcription start sites (TSSs ±500 bp) of RefSeq genes [33] and are referred to as promoter FAIRE peaks (Figure S1A), while 72% were located outside known TSSs, and are referred to as non-promoter FAIRE peaks. Notably, only 8% of the non-promoter FAIRE peaks were located in a −5 kb proximal promoter region while the majority of non-promoter FAIRE peaks were located in introns and distal regions (Figure S1A). Average profiling revealed that a FAIRE signal, H3K4me3

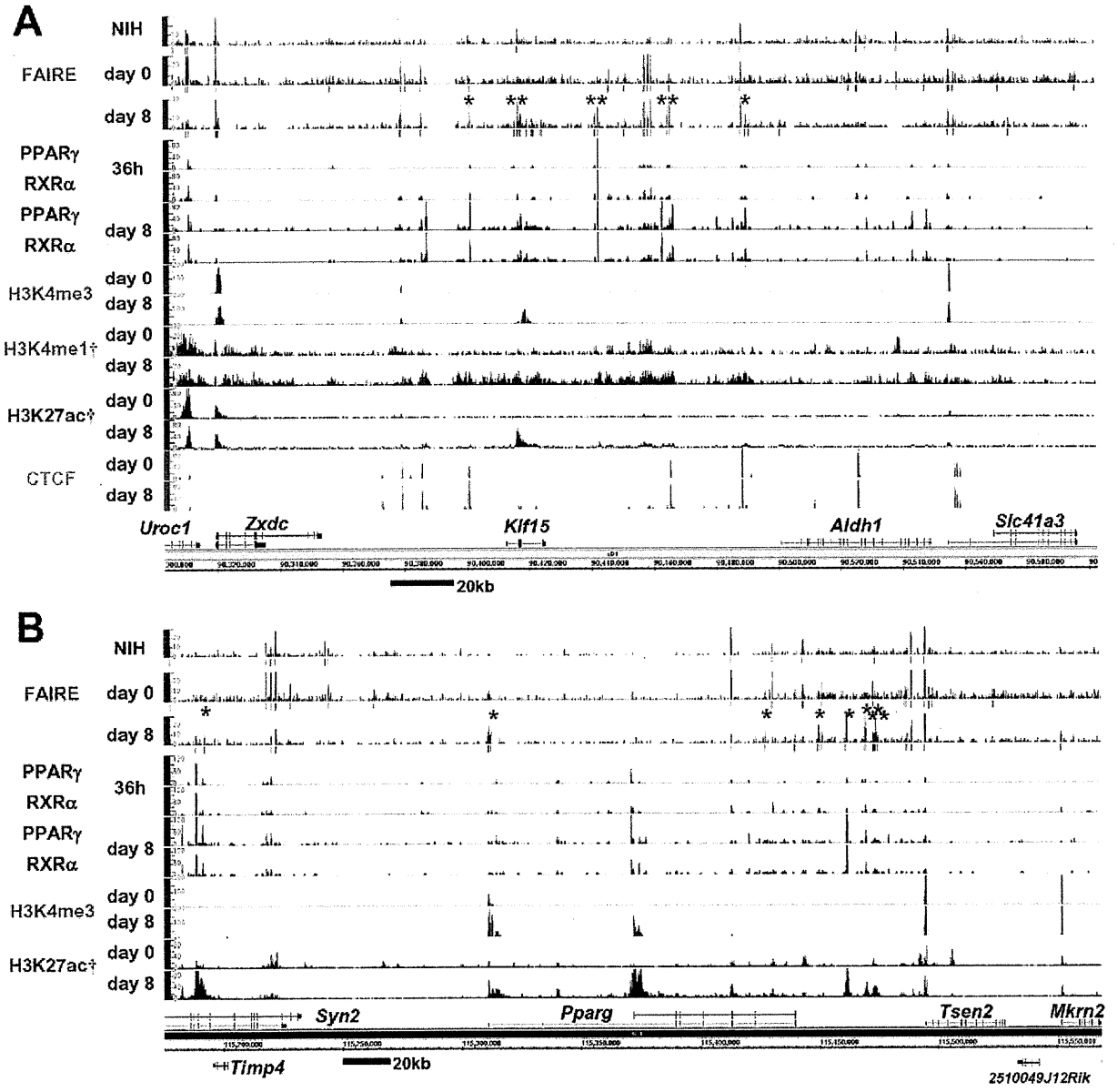

Figure 1. Genome-wide profiling of open chromatin regions by FAIRE-seq in 3T3-L1 adipocyte differentiation. Open chromatin regions detected by FAIRE-seq were observed in both promoter and non-promoter regions. The non-promoter FAIRE peaks were associated with the binding of PPARγ/RXRα or CTCF, and with the enhancer signature H3K4me1(+)/me3(−) and H3K27ac modification—while the promoter FAIRE peaks were associated with H3K4me3 and H3K27ac modification. Bars below the FAIRE peaks data represent statistically significant FAIRE positive peaks (FDR<10^{-4}). Red asterisks indicate the adipocyte-specific FAIRE peaks on day 8 (see Figure 2B for definition). Multiple adipocyte-specific FAIRE peaks were located within genomic regions near *Klf15* (A) and *Pparg* (B) in 3T3-L1 adipocytes. Data marked (†) were obtained from Mikkelsen et al. [28] (GSE20752).
doi:10.1371/journal.pgen.1002311.g001

and histone H3 lysine 27 acetylation (H3K27ac) were observed at TSSs of actively transcribed genes (Figure S1B and S1D). On the other hand, non-promoter FAIRE peaks were accompanied by monomodal enrichment of H3K4me1 and were devoid of H3K4me3 enrichment, a condition described as the signature of enhancers [34,35] (Figure S1D). CTCF binding sites are important in insulator function and high-order chromatin structure [31]. The CTCF binding sites in our study (day 0 or day 8) were largely overlapped by those in a study by Mikkelsen (day 0 or day 7) [28] (86.3% and 88.5%, respectively). CTCF binding accounted for about one fifth of either the promoter or non-promoter FAIRE peaks (Figure 1 and Figure S1C). Collectively, these data suggest that the open chromatin sites identified by FAIRE-seq show characteristics of regulatory elements such as promoter, enhancer and insulator.

Analysis of Differentiation-Dependent Non-Promoter FAIRE Peaks

We next compared the FAIRE peaks in 3T3-L1 cells on day 0 and day 8 and in NIH-3T3 cells. The promoter FAIRE peaks were relatively constant among the three groups. Over 70% of

those peaks on day 0 and day 8 3T3-L1 cells and in NIH-3T3 cells were shared by all three groups (Figure 2A). In contrast, non-promoter FAIRE peaks showed dynamic change. The three groups shared only 25%, 45%, and 26% of non-promoter FAIRE peaks in, respectively, day 0 and day 8 3T3-L1 cells and NIH-3T3 cells. This contrasts with an invariable biding pattern of CTCF in

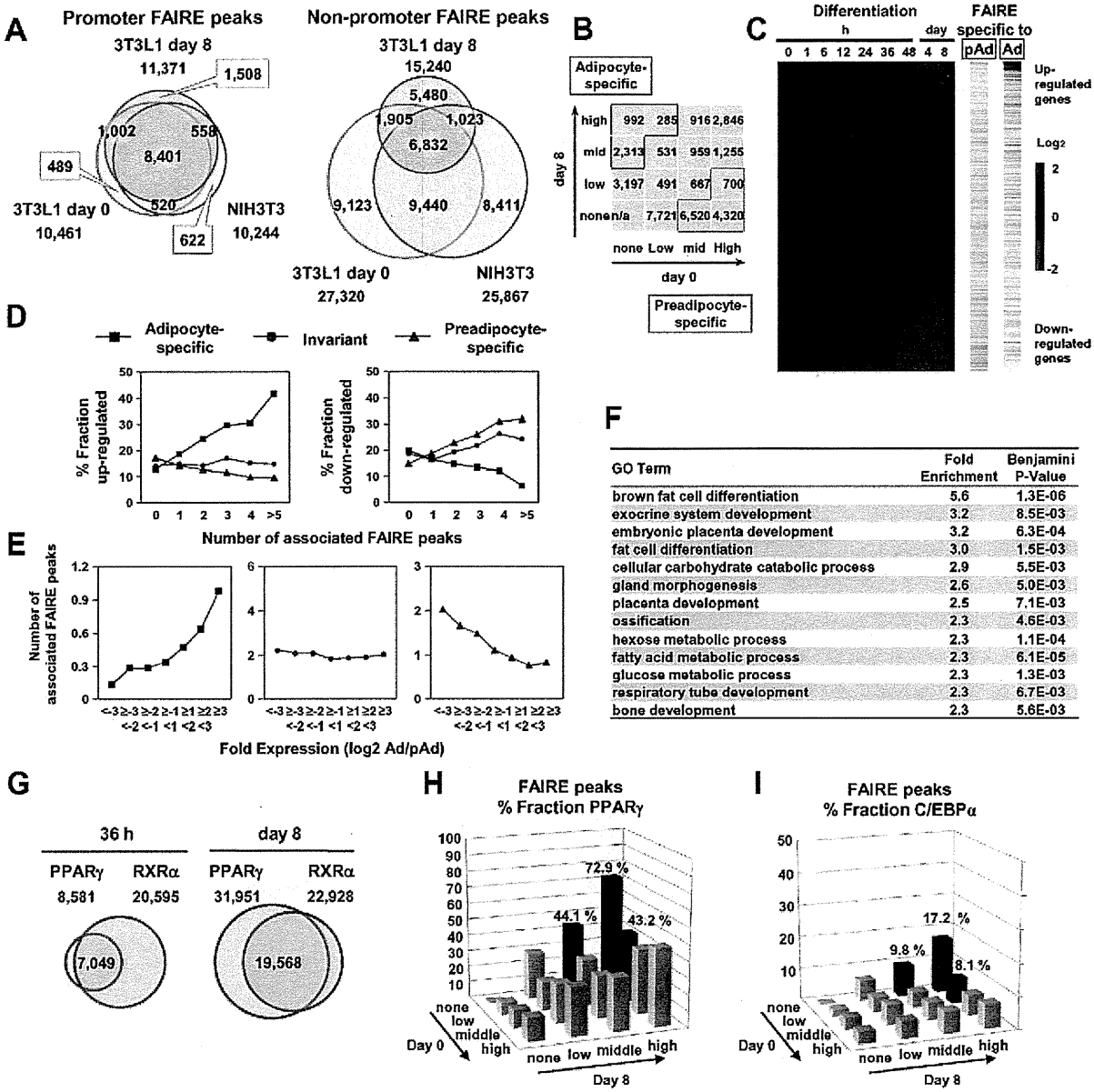

Figure 2. Cell type– and differentiation-dependent FAIRE peaks. (A) Venn diagrams comparing the FAIRE peaks among 3T3-L1 (day 0), 3T3-L1 (day 8) and NIH-3T3 at promoter (+/−500 bp from RefSeq TSS) and non-promoter regions. The promoter FAIRE peaks were relatively constant among the three cell groups while the non-promoter FAIRE peaks were highly variable. (B) The FAIRE peaks in 3T3-L1 (day 0 or day 8) were divided into tertiles by peak height and adipocyte- (red boxes) and preadipocyte-specific (green boxes) FAIRE peaks, and were defined as indicated. (C) A heat map showing enrichment of the adipocyte- and preadipocyte-specific FAIRE peaks in the vicinity (+/−25 kb from TSS) of genes up-regulated or down-regulated during differentiation. The horizontal bars in the two right panels indicate each gene with Ad or pAd FAIRE peaks in the vicinity (+/−25 kb from TSS). (D) Fractions of genes that were up-regulated (left) or down-regulated (right) more than two-fold during differentiation among genes that had the indicated number of adipocyte- (red), preadipocyte-specific (green) or invariant (blue) FAIRE peaks. (E) The number of the adipocyte- (red), preadipocyte-specific (green) or invariant (blue) FAIRE peaks associated with genes that were stratified by the ratio of the expression levels between preadipocytes and adipocytes. Each FAIRE peak was defined as associated with the nearest gene in analyses (D) and (E). (F) Ontology analysis by DAVID of genes associated (+/−25 kb from TSS) with adipocyte-specific FAIRE peaks [13]. (G) Venn diagrams showing the numbers and overlap of the binding sites for PPARγ and RXRα in 3T3-L1, day 0 and day 8. (H, I) Fractions of the non-promoter FAIRE peaks that overlap PPARγ binding sites (day 8) (H) or C/EBPα binding sites (Schmidt et al., GSE27450 [86]) (I). PPARγ and C/EBPα represented 45.3% and 11.7% of the adipocyte-specific FAIRE peaks (average of red bars).

doi:10.1371/journal.pgen.1002311.g002

the non-promoter regions; in 3T3-L1 cells, 89.5% of the non-promoter CTCF binding sites on day 0 overlapped those on day 8. What's more, a significant proportion of the non-promoter FAIRE peaks were cell type–specific (Figure 2A), implying the role of non-promoter regulatory elements in cell type–specific transcriptional regulation. We divided the non-promoter FAIRE peaks in day 0 and day 8 3T3-L1 cells into tertiles by FAIRE signal intensity, and defined adipocyte- or preadipocyte-specific FAIRE peaks as indicated by red or green boxes in the 4-by-4 table in Figure 2B. By this definition, we judged each non-promoter FAIRE peak as adipocyte-specific, preadipocyte-specific or invariant (Figure 2B). Figure 1, Figures S2 and S3 show examples of adipocyte-specific non-promoter FAIRE peaks (indicated by asterisks) in loci near *Klf15*, *Pparg*, *Cebpa* [16,20], *Mgll* [36], *Srebf1* and *cidec* [37]—all of which are abundantly expressed in adipose tissue and induced during adipocyte differentiation (data not shown). Remarkably, multiple adipocyte-specific FAIRE peaks existed in the vicinity of these genes and included introns and downstream regions (Figure 1, Figures S2 and S3).

To determine whether non-promoter FAIRE peaks were functionally associated with cell type–specific gene expression, we analyzed the relationship between the presence of the adipocyte- or preadipocyte-specific non-promoter FAIRE peaks and the change in gene expression during adipocyte differentiation. Those FAIRE peaks were enriched in the vicinity of genes, expression levels of which were highly induced or suppressed during adipocyte differentiation (Figure 2C). Importantly, as the number of the adipocyte-specific FAIRE peaks associated with a gene increased, the fraction of up- or down-regulated genes increased or decreased, respectively (Figure 2D, red lines), while as the number of associated preadipocyte-specific FAIRE peaks increased, the fraction of up- or down-regulated genes decreased or increased, respectively (Figure 2D, green lines). Conversely, the more robust the induction of the expression level of a gene during adipocyte differentiation, the greater the numbers of adipocyte-specific FAIRE peaks associated with the gene (Figure 2E, red line). In contrast, the more robust the reduction of the expression levels of a gene during adipocyte differentiation, the greater the numbers of associated preadipocyte-specific FAIRE peaks that were associated (Figure 2E, green line). Invariant FAIRE peaks were associated specifically with neither up- nor down-regulated genes (Figure 2E, blue line). We next employed a gene ontology (GO) analysis tool (DAVID) [38] to determine what kind of biological processes were associated with genes bound by the adipocyte-specific FAIRE peaks. We found that biological processes (e.g., adipocyte differentiation) were significantly enriched compared with the genomic background (Figure 2F). It was of interest that embryonic placenta development—for which PPARγ is critical [13,14,15]—was enriched (Figure 2F). Together, these data highlight the role of the cell type–specific non-promoter open chromatin sites detected by FAIRE-seq in differentiation-dependent transcriptional regulation.

Analysis of Binding Sites for PPARγ and RXRα in 3T3-L1 Adipocytes

PPARγ is key regulator of adipocyte development [16,20]. To elucidate the contribution of PPARγ to adipocyte-specific transcriptional regulation, we conducted ChIP-seq analyses using antibodies specific for either PPARγ or RXRα [24] in 3T3-L1 adipocytes at 36 hours and day 8 after induction of differentiation. The number of PPARγ binding sites increased during differentiation while that of RXRα binding sites remained virtually constant (Figure 2G). Significant overlap between the PPARγ and RXRα binding sites was consistent with the heterodimer formation of PPARγ and RXRα [21,39] (Figure 2G). Microarray and GO analysis revealed that the PPARγ binding sites were enriched in the vicinity of genes up-regulated by adipocyte differentiation (Figure S4B) and the bound genes were associated with adipocyte differentiation and lipid metabolism (Figure S4C). Using MEME [40], we performed de novo motif analysis of genomic regions bound by PPARγ, and found that the AGGTCA-n-AGGTCA (called DR-1) shown was the most over-represented one (E-value 1.3×10^{-055}) (Figure S4A). An extension AGT 5′ outside of DR-1 appeared to correspond to the direct interaction between the DNA and the hinge region between the DNA-binding domain and the ligand-binding domain [41].

As shown in genomic loci (Figure 1, Figures S2 and S3), a significant proportion of adipocyte-specific non-promoter FAIRE peaks overlapped the PPARγ/RXRα binding sites. To determine the contribution of PPARγ to the adipocyte-specific open chromatin regions, we calculated percent fractions of the FAIRE peaks that were stratified by FAIRE signal in 3T3-L1 on day 0 and day 8 (Figure 2B) —and that overlapped either the PPARγ binding sites (Figure 2G) or C/EBPα binding sites in 3T3-L1 reported by Schmidt et al. [42]. Both PPARγ and C/EBPα binding sites were enriched in the fractions of adipocyte-specific FAIRE peaks (Figure 2H and 2I), and they respectively accounted for 45.3% and 11.7% of the adipocyte-specific FAIRE peaks (averages of the red bars in Figure 2H and 2I). These data support the role of PPARγ and C/EBPα as primary transcription factors that drive adipocyte-specific gene expression—although they may not explain all of it.

Clustering of Multiple Adipocyte-Specific Non-Promoter FAIRE Peaks and the PPARγ Binding Sites

Genes that were highly induced by adipocyte differentiation often harbored multiple adipocyte-specific FAIRE peaks and/or PPARγ binding sites in their vicinity, as suggested by the linear correlation between the number of the associated adipocyte-specific FAIRE peaks and the robustness of the induction of the gene by adipocyte differentiation (Figure 2D and 2E). (See Figure 1, Figures S2 and S3 for representative genes.) To determine whether these multiple regions have functional regulatory elements, we selected AdipoR2 [43,44]. Although AdipoR2 was regulated by PPARγ and PPARα ([45] and data not shown), conventional −2 kb promoter studies failed to identify the response element [46]. Our ChIP-seq analysis revealed a cluster of multiple PPARγ/RXRα binding sites in the intron 1, downstream of the TSS of AdipoR2 (Figure S2B, arrow heads). We identified putative DR-1 motifs in these biding sites (Figure 3A) and tested them by gel-shift assay and luciferase assay. These motifs were indeed bound by the PPARγ/RXRα heterodimer, and were functional in the luciferase assay (Figure 3B and 3C), suggesting the functionality of these elements and the advantage of a genome-wide approach over the conventional "promoter-bashing" approach to identifying such response elements.

Recent genome-wide studies revealed clustering of open chromatin regions detected by Dnase I hypersensitivity assay or by FAIRE in the genomes of CD4+ T cells [47], pancreatic islet cells [10,48] and binding sites for certain transcription factors [49])—certainly the PPARγ binding sites and adipocyte-specific FAIRE peaks in our analyses tended to form clusters as indicated by an additional peak in distribution histograms of the distance to the nearest peak among the PPARγ binding sites or the adipocyte-specific FAIRE peaks (Figure 4A). We calculated the total number of PPARγ binding site clusters for different window sizes and compared them with a random data set comprised of the same number of sites (Figure 4B). The PPARγ binding sites had a

A

Fabp4 (aP2) (-5.4 kb)		
ARE7	+	CTTACTGGATCAGAGTTCACTAGTG
near ARE7	-	AGTAAGAAGGCAAATGTCAGGCATC
ARE6	-	CTCTCTGGGTGAAATGTGCATTTCT
Adipor2 peak 1 (+20 k)		
PPRE #1	+	TGTGCAGGGACAAATGCCAAGCCCC
PPRE #2	-	CCCATGAAGGCAGAGGTTATGGGCA
Adipor2 peak 2 (+17 k)		
PPRE #3	+	TGTGCTAGGGTAAAGGTGGCACAAA
PPRE #4	-	CATTGTAGGTCAAGGGTTTTGTGGC
Adipor2 peak 3 (+8 k)		
PPRE #5	+	TTTCCTGGCACACAGGTCTCCAGAC
PPRE #6	-	AGAATTGGGGCAGAGGGAAACTGTT
Adipor2 peak 4 (+6 k)		
PPRE #7	+	TTTGCCAGGGAAATGGTCACAGAGT
PPRE #8	-	CTATGTAGGCCAGAGGGTGATCTGC

B

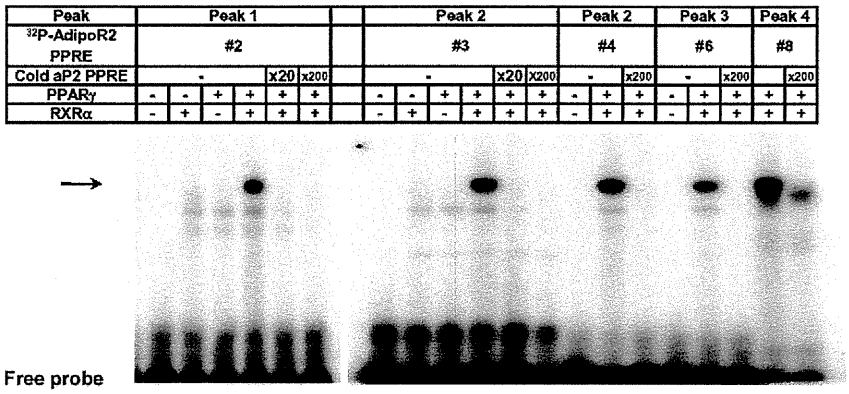

C

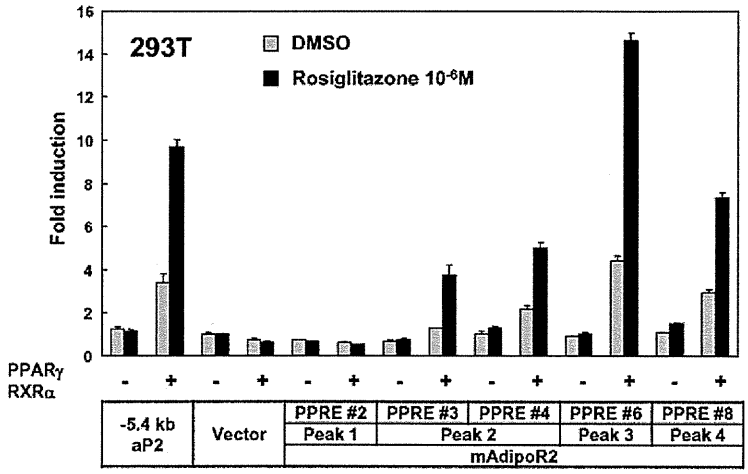

Figure 3. Identification of functional regulatory elements in the intron 1 of *Adipor2*. The PPARγ binding sites in the *Adipor2* gene locus (Figure S2B, arrow heads) were analyzed. (A) Putative DR-1 motifs (PPAR response elements or PPREs) in the regions. ARE6 and ARE7 in the −5.4 kb promoter upstream of *Fabp4*(aP2) were previously identified PPREs [87]. (B) Gel shift assay showing binding of the PPARγ/RXR heterodimer to the motifs. An arrow indicates the PPARγ/RXRα heterodimer bound by radiolabeled probe. Competition by cold oligos showed the specificity of the binding. (C) Luciferase reporter assay in HEK293T cells. Most of the motifs inserted into reporter vectors with the tk minimal promoter responded to over-expressed PPARγ/RXRα and stimulation with its synthetic ligand, rosiglitazone. The −5.4 kb promoter of PPARγ target gene *Fabp4* (aP2) [84] was included as a positive control.

doi:10.1371/journal.pgen.1002311.g003

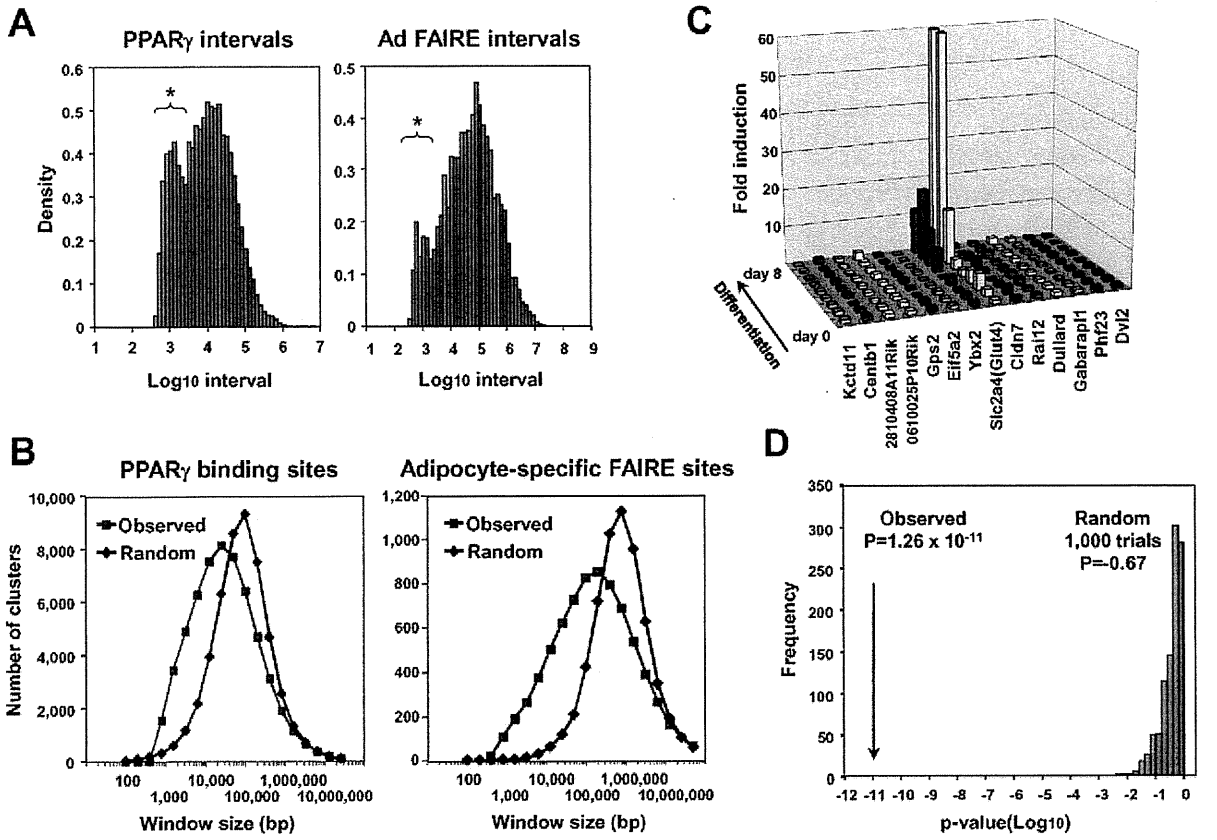

Figure 4. Statistical analyses for clustering of adipocyte-specific FAIRE peaks and PPARγ binding sites and co-regulation of neighbor genes during adipogenesis. (A) Histogram showing distribution of intervals (defined as distances to the nearest neighbor sites) among all PPARγ peaks (left) and among the adipocyte-specific FAIRE peaks (right). Note that there was increased occurrence of sites separated by short intervals (indicated by asterisks). See [48] for details of the method. (B) Clustering analysis of the PPARγ binding sites and the adipocyte-specific FAIRE peaks by counting the total number of clusters (defined as more than two peaks) determined for windows with indicated width. The PPARγ binding site or adipocyte-specific FAIRE peak clusters occurred more frequently in the observed data set than in random data with the same number of sites. The difference in the number of clusters was observed at window sizes ranging from 800 bp to 30~100 kb compared with the random sample. See reference [47] for details of the method. (C) Microarray analysis showing both *Slc2a4 (Glut4)* and *Ybx2* included in the adipocyte-specific FAIRE peak cluster (Figure S2C) co-regulated during differentiation. (D) Neighbors of highly induced genes (>10 fold) were more likely to be up-regulated over three fold (18%, or 112 of 618 neighbors) than the 2,012 of 21,343 total genes (9%) that were up-regulated over three fold ($p = 1.26 \times 10^{-12}$, one-sided Fisher test). Neighbors of randomly selected genes were not significantly up-regulated ($p = -0.67$, average of 1,000 trials). See reference [50] for method.

doi:10.1371/journal.pgen.1002311.g004

significantly higher number of clusters in a window size raging from 800 bp to ~30 kb. Similar results were obtained for the adipocyte-specific FAIRE peaks (Figure 4A and 4B).

On the other hand, multiple genes involved in adipocyte function [55,56,57] were often co-regulated in certain genomic regions that harbor clusters of adipocyte-specific regulatory elements (see Figure S2C, Figure 4C, and Figure S5). We therefore statistically tested—method in reference [50]—to see if neighboring genes tended to be co-regulated during adipocyte differentiation, and found that neighbors of highly induced genes (>10 fold) were indeed more likely to be up-regulated over three fold (18%, or 112 of 618 neighbors) than the 2,012 of 21,343 total genes (9%) that were up-regulated over three fold ($P = 1.26 \times 10^{-12}$, one-sided Fisher test). Neighbors of randomly selected genes were not significantly up-regulated ($p = -0.67$, average of 1,000 trials, Figure 4D). Together, these data suggest that the transcriptional regulation of genes during adipocyte differentiation involves multiple adipocyte-specific regulatory elements—which tend to form clusters—and that co-regulation of neighboring genes often occurs during adipocyte differentiation.

Sequence Motif Analyses of DNA Sequences of the Adipocyte-Specific Non-Promoter FAIRE Peaks

Next, we performed enrichment analyses of known motifs using AME in the MEME suite and the TRANSFAC [51] and JASPER [52] motif databases to identify motifs enriched in either adipocyte- or preadipocyte-specific FAIRE peaks compared with the background (statistical values shown as corrected p-value in Figure 5). We also determined the enrichment ratio (Ad/pAd) by calculating the ratio of occurrence of a motif in the adipocyte-specific FAIRE peaks and in the preadipocyte-specific FAIRE peaks as described in reference [28]. Using both parameters, we obtained motifs that had been significantly enriched in either kind of FAIRE peak and that occurred in significantly different number. Figure 5 shows the top of the list of TRANSFAC motifs enriched in the adipocyte- and preadipocyte-specific FAIRE

TRANSFAC motifs

Adipocyte-specific FAIRE peaks

Motif	Name	Corrected p-value	Enrich-ment Ratio (Ad/pAd)	Logo
M00193	NF-1	7.9E-27	1.60	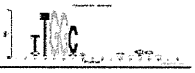
M01196	CTF1 (NF-1)	5.1E-22	1.55	
M01100	LRF	2.6E-20	1.65	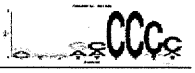
M00528	PPAR	2.7E-12	2.14	
M01728	EAR2	1.2E-09	1.47	
M01031	HNF4 (PPAR)	3.8E-08	2.06	
M01772	C/EBP	1.7E-07	2.69	
M00109	C/EBPbeta	3.1E-07	1.51	
M00121	USF/Tcf4 Max/c-Myc	6.3E-07	1.52	
M00491	MAZR	2.1E-05	1.29	

Preadipocyte-specific FAIRE peaks

Motif	Name	Corrected p-value	Enrich-ment Ratio (Ad/pAd)	Logo
M00925	AP-1	1.1E-221	0.07	
M00495	Bach1	1.2E-183	0.09	
M00037	NF-E2	2.3E-84	0.23	
M00769	AML	1.8E-15	0.53	
M00984	PEBP	3.1E-15	0.49	
M01305	TEF	2.7E-13	0.44	
M00284	TCF11:MafG	5.2E-12	0.30	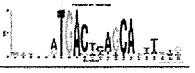
M00115	Tax/CREB	2.2E-06	0.47	
M01080	CBF	1.1E-05	0.50	
M01666	STAT4	3.6E-02	0.59	

Figure 5. Known motif enrichment analysis of adipocyte- or preadipocyte-specific FAIRE peaks (TRANSFAC motifs). Enrichment analysis of the adipocyte- (left) and the preadipocyte-specific (right) FAIRE peaks for known motifs in the TRANSFAC database (Release 2010.4) performed by using AME in the MEME suite. After removing repeat regions with RepeatMasker [83], DNA sequences from the center 150 bp regions of the top 2,000 cell type–specific FAIRE peaks were analyzed (p-value report threshold : 0.05). Motif enrichment ratios (Ad/pAd FAIRE) for motifs in the TRANSFAC database were also determined by a method described in reference [28]. Motifs with an enrichment ratio greater than 1.20 (for the adipocyte-specific FAIRE peaks, left) or less than 0.833 (for the preadipocyte-specific FAIRE peaks, right) are shown in the table. See "Materials and Methods" for details.
doi:10.1371/journal.pgen.1002311.g005

peaks. The motifs for PPARγ (and other DR1 motifs) and C/EBPs were among the list, consistent with their critical roles in adipogenic transcription. Motif analyses using the JASPER motif database showed enrichment of the motifs for PPARγ, C/EBPs and the motif for Zfp423, a recently identified adipogenic regulator [53] (Figure S6). Motif analyses of the preadipocyte-specific FAIRE peaks showed significant enrichment of a motif for AP-1, a downstream transcription factor complex of the growth factor/MAP kinase signaling pathways, which include epidermal growth factor and c-Jun N-terminal kinases, known inhibitors of adipogenesis [54,55] (Figure 5 and Figure S6). We also performed de novo motif analysis (MEME) [40] of the adipocyte-specific FAIRE peaks, and observed significant enrichment of motifs that corresponded to those for PPARγ and C/EBPs (Figure S7). Together, these instances of enrichment of known regulators indicate the validity of this approach.

Identification of NFI Family Transcription Factors as Novel Regulators of Adipocyte Differentiation

There were several other motifs for transcription factors, their functions not previously linked to adipocyte differentiation (Figure 5, Figures S6 and S7). We focused on a motif for the NFI family transcription factors. The murine NFI family consists of NFIA, NFIB, NFIC and NFIX, and was identified as a site-specific DNA-binding protein that bound to the adenovirus origin of replication [56]. It forms a dimer to bind to the symmetric consensus sequence TTGGC(N5)GCCAA [57]. We first examined the expression change of these factors in in vitro adipocyte differentiation and found that the expression of NFIA and NFIB were significantly induced during differentiation of 3T3-L1 and of another adipogenic cell line, 3T3-F442A (Figure 6A and 6C). Consistent with this pattern, both NFIA and NFIB were highly expressed in a variety of adipose tissue depots in addition to the brain (Figure 6B). We next examined the effect of siRNA knockdown of NFIA and NFIB on adipogenic gene regulation and adipocyte differentiation (Figure 6C). Interestingly, induction of the expression of the adipogenic transcription factors PPARγ and C/EBPα and of downstream genes was significantly suppressed by siRNA knockdown of either NFIA or NFIB (Figure 6C). Consistent with the gene expression change, we observed significant reduction of lipid accumulation as judged by oil red O staining, suggesting physiological roles for NFIA and

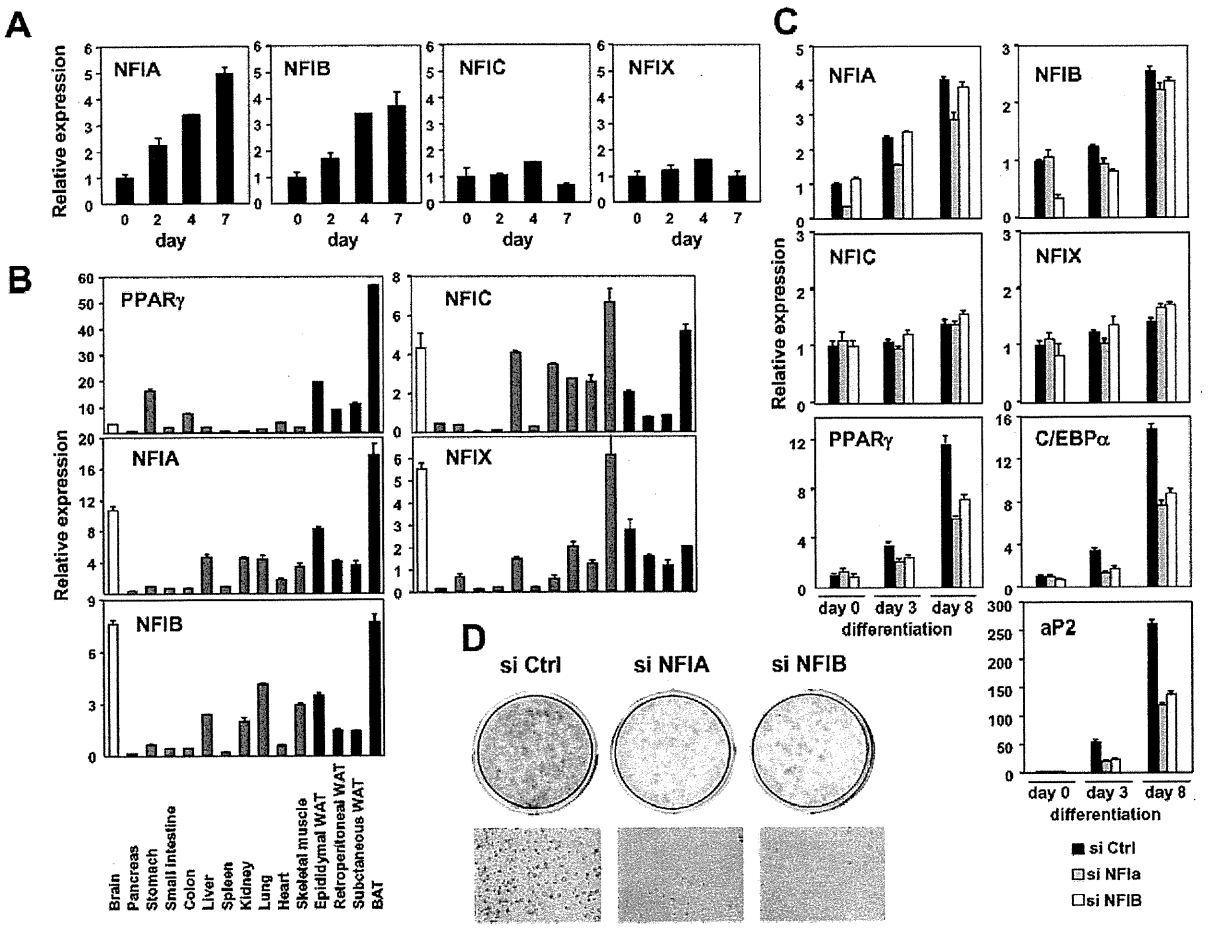

Figure 6. NFIA and NFIB are novel regulators of adipocyte differentiation. (A) Transcriptional regulation of NFI transcription factors during adipocyte differentiation (3T3-F442A). (B) Tissue distribution of the NFI family genes. Expression levels relative to 36B4 in various tissues were determined by qPCR. (C, D) Effects of siRNA-mediated knockdown of NFIA and NFIB on adipogenic gene expression (C) and lipid accumulation in 3T3-L1 adipocytes judged by oil red O staining (D). Knockdown of either NFIA or NFIB resulted in suppression of the induction of PPARγ, C/EBPα and the PPARγ target gene, aP2, as well as increase in lipid accumulation during adipocyte differentiation.
doi:10.1371/journal.pgen.1002311.g006

NFIB in adipocyte differentiation (Figure 6D). We confirmed the effect of NFIA and NFIB knockdown on adipogenesis by using independent pooled siRNA (Figure S8).

We next asked whether overexpression of these factors influence adipocyte differentiation. We amplified NFIA and NFIB coding sequences from cDNA prepared from adipocytes, and cloned them into retroviral pMXs-puro vectors. We also made a dominant negative NFIA that lacks the C-terminal transactivation/repression domain (NFIA-DN) [58]. Overexpression of NFIA—but not NFIA-DN or NFIB—resulted in robust induction of PPARγ, C/EBPα and aP2 (Figure 7A) at a basal state. Surprisingly, the induction of these factors was robust enough to make the cells to form lipid droplets visible and stainable by oil red O even before initiation of differentiation by the DMI (dexamethasone, IBMX and insulin) treatment (Figure 7B and 7C). However, after the DMI treatment, NFIA-expressing cells were overtaken by control cells, and on day 7, NFIA and NFIB overexpressing cells showed attenuated differentiation (Figure 7D and 7E). We speculate that this was caused by secondary effects of overly strong overexpression levels (>30 fold, Figure 7A). Almost complete suppression of adipogenesis by NFIA-DN overexpression was consistent with the results of knockdown experiments (Figure 6, Figure 7D and 7E). Nevertheless, the robust induction of PPARγ, C/EBPα and aP2 by NFIA overexpression at the basal state implies direct action of NFIA on transcriptional control of these factors.

To dissect the mechanism by which NFIs regulate PPARγ, C/EBPα and aP2, we examined DNA sequences of the adipocyte-specific FAIRE peaks and/or the PPARγ binding sites in the vicinity of these factors and found that some of them have NFI binding motifs as listed in Figure 8A. ChIP analysis using an anti-NFI antibody confirmed actual binding of NFI to these sites (Figure 8B and 8C). We extended this experiment by counting NFI motifs in the FAIRE peaks on a genome-wide scale. Interestingly, percent fractions of genes harboring NFI binding motifs in the FAIRE peaks were higher when the genes were bound by PPARγ and induced during differentiation (Figure 8D), indicating a significant degree of specificity for the NFI's action on the adipogenic transcriptional program.

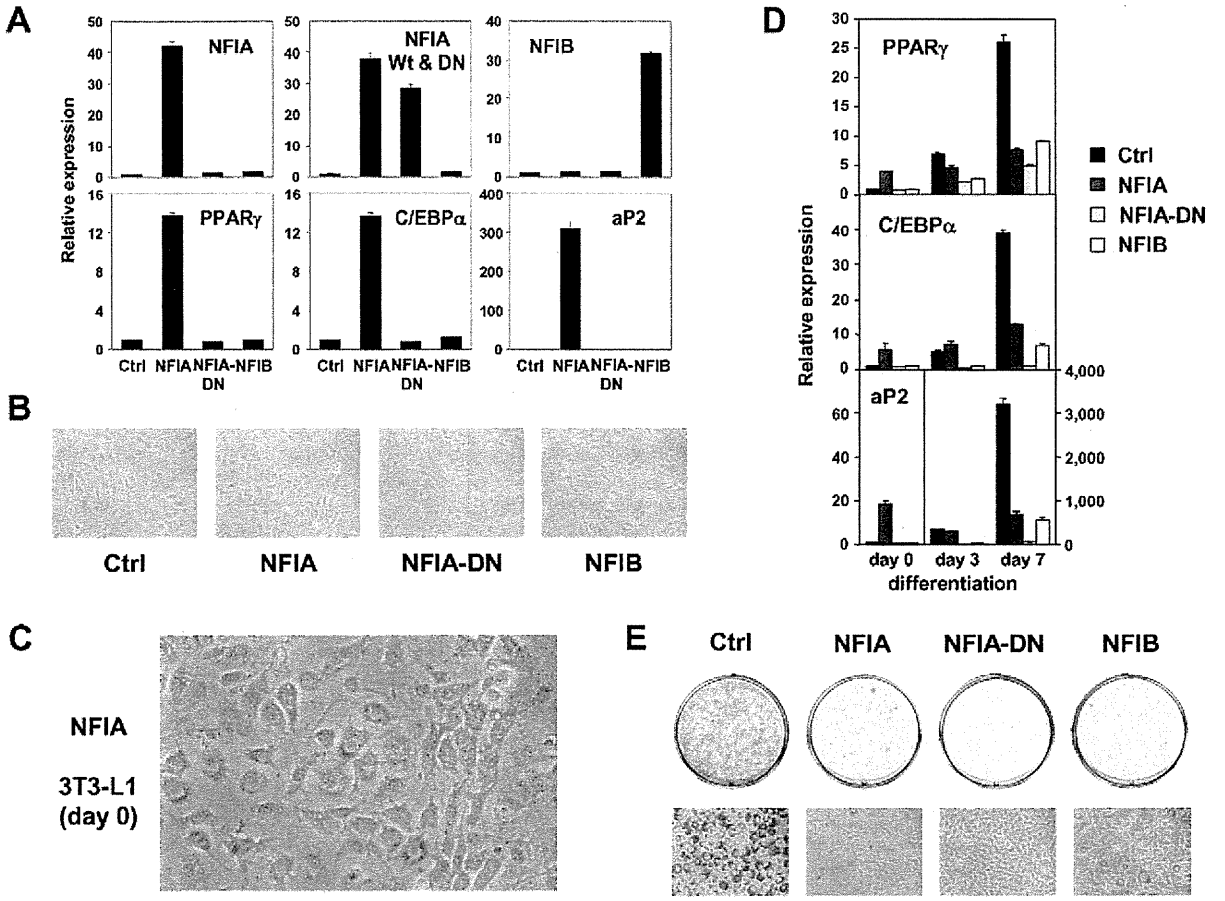

Figure 7. Overexpression of NFIA, NFIB, and dominant negative NFIA in 3T3-L1 cells. (A) Expression analysis of overexpressed NFI factors (upper panel) and adipogenic PPARγ, C/EBPα and aP2 (lower panel). Note, overexperssion of NFIA resulted in a robust induction of adipogenic factors. (B) Microscopic pictures of 3T3-L1 cells overexpressing NFI factors at confluence stained by oil red O (day 0). (C) Close examination of NFIA-overexpressing cells revealed formation of lipid droplets without adipogenic stimulus before differentiation. (D) Time course of expression levels of PPARγ, C/EBPα and aP2 during differentiation. Note, the induction of these genes by NFIA overexpression was overtaken by that of control cells, and on day 7, NFIA and NFIB overexpressing cells showed attenuated differentiation. Dominant negative NFIA showed almost complete suppression. (E) Oil red O staining of 3T3-L1 overexpressing NFI factors on day 7.
doi:10.1371/journal.pgen.1002311.g007

Collectively, we demonstrated that the combination of FAIRE-seq and computational motif analyses is useful in identifying novel regulators of adipocyte differentiation.

Comparison of FAIRE Peaks between Undifferentiated 3T3-L1 and NIH-3T3 Cells

The 3T3-L1 adipogenic cell line was established by isolating clonal sublines of mouse fibroblast line 3T3 [59]. Lastly, we compared FAIRE peaks between 'undifferentiated' 3T3-L1 and NIH-3T3 cells. As shown in Figure 2A, a substantial proportion of FAIRE peaks was unique to either 3T3-L1 or NIH-3T3 cells. We defined non-promoter FAIRE peaks as specific to 3T3-L1and NIH-3T3—as we did for the adipocyte- or preadipocyte-specific FAIRE peaks in Figure 2B. The 3T3-L1- or NIH-3T3-specific FAIRE peaks were enriched in the vicinity of genes whose expression levels were higher in 3T3-L1 or NIH-3T3, respectively (Figure S9A). Motif analysis of the 3T3-L1-specific FAIRE peaks showed that the binding motif for EBF (Figure S9B) had the highest enrichment ratio (1.81) and a statistically significant p-value of 3.9E-3. Although the p-value of the motif for PPARγ/RXR did not reach statistical significance, that motif had an enrichment ratio of 1.84. These two factors were among the handful that were proven to transform NIH-3T3 cells into adipocytes when ectopically introduced [16,60].

Discussion

We demonstrated that genome-wide mapping of open chromatin regions by FAIRE-seq is a simple, accurate method that allows a snapshot view of regulatory elements in the genome. Although open chromatin regions detected by FAIRE-seq include promoters of transcribed genes, enhancers and insulators, open chromatin regions that vary in two different conditions likely contain regulatory elements that play roles in the specific biological process. By comparing open chromatin regions in preadipocytes and adipocytes, we identified the adipocyte- and preadipocyte-specific FAIRE peaks in the genome. Functionally, we demonstrated that the adipocyte-specific FAIRE peaks were associated with genes up- regulated by adipogenesis while the preadipocyte-specific FAIRE peaks were associated with genes down-regulated by adipogenesis (Figure 2C, 2D and 2E). Adipocyte gene